Manuscript Details

Manuscript number	ICARUS_2016_366_R3
Title	Mesospheric CO2 ice clouds on Mars observed by the Planetary Fourier Spectrometer onboard Mars Express
Article type	Research paper

Abstract

We have investigated mesospheric CO2 ice clouds on Mars through analysis of near-infrared spectra acquired by Planetary Fourier Spectrometer (PFS) onboard the Mars Express (MEx) from MY 27 to MY 32. With the highest spectral resolution achieved thus far in the relevant spectral range among remote-sensing experiments orbiting Mars, PFS enables precise identification of the scattering peak of CO2 ice at the bottom of the 4.3 μm CO2 band. A total of 111 occurrences of CO2 ice cloud features have been detected over the period investigated. Data from the OMEGA imaging spectrometer onboard MEx confirm all of PFS detections from times when OMEGA operated simultaneously with PFS. The spatial and seasonal distributions of the CO2 ice clouds detected by PFS are consistent with previous observations by other instruments. We find CO2 ice clouds between Ls = 0° and 140° in distinct longitudinal corridors around the equatorial region (± 20°N). Moreover, CO2 ice clouds were preferentially detected at the observational LT range between 15–16 h in MY 29. However, observational biases prevent from distinguishing local time dependency from inter-annual variation. PFS also enables us to investigate the shape of mesospheric CO2 ice cloud spectral features in detail. In all cases, peaks were found between 4.240 and 4.265 μm. Relatively small secondary peaks were occasionally observed around 4.28 μm (8 occurrences). These spectral features cannot be reproduced using our radiative transfer model, which may be because the available CO2 ice refractive indices are inappropriate for the mesospheric temperatures of Mars, or because of the assumption in our model that the CO2 ice crystals are spherical and composed by pure CO2 ice.

Keywords	Mars; Mars, atmosphere; Mars, climate; Infrared observations; Spectroscopy

Corresponding Author	SHOHEI AOKI
Order of Authors	SHOHEI AOKI, Yuki Sato, Marco Giuranna, Paulina Wolkenberg, Takao Sato, Hiromu Nakagawa, Yasumasa Kasaba

Suggested reviewers	Erdal Yiğit, Francisco Gonzalez-Galindo, Anni Maattanen, Constantino Listowski, Ruth Signorell, Mathieu Vincendon

Submission Files Included in this PDF

File Name [File Type]

REPLY TO COMMENTS FROM EDITOR AND REVIEWERS_Revise3_final.docx [Response to Reviewers]

Highlights.doc [Highlights]

manuscript_Revise3_final.docx [Manuscript File]

Figure1.pdf [Figure]

Figure2.pdf [Figure]

Figure3a.jpg [Figure]

Figure3bc.pdf [Figure]

Figure4.pdf [Figure]

Figure5.pdf [Figure]

Figure6.pdf [Figure]

Figure7.pdf [Figure]

FigureA1.pdf [Figure]

To view all the submission files, including those not included in the PDF, click on the manuscript title on your EVISE Homepage, then click 'Download zip file'.

REPLY TO COMMENTS FROM EDITOR AND REVIEWERS

3 October 2017

Dear Editor and Reviewers,

The authors thank you very much for many valuable comments on the manuscript. Please find the revised manuscript entitled "Mesospheric CO_2 ice clouds on Mars observed by the Planetary Fourier Spectrometer onboard Mars Express". Based on the comments by the reviewers, moderate amounts of sentences have been rewritten and added. In the manuscript, the revised parts are written in red.

The main changes in this revision are as follows:

1. Discussion on the possible contribution from the global dust storm to the formation of the CO_2 ice clouds:

Both reviewers pointed out that we did not have solid cases to establish the hypothesis that an increase of small dust particles suspended at mesospheric altitudes after the occurrence of a global dust storm could contribute the increase of CO_2 clouds detections in MY 29. We have revisited that and have agreed with the reviewers. In the revised manuscript, we shorten the discussion and also remove the Appendix B. In the new statement, we simply describe that Listowski et al. (2014) discussed possible contribution from a dust storm to the formation of the mesospheric CO_2 ice clouds and they did not support that the cloud nuclei are brought by the global dust storm.

The revised text (Lines 277-284): "*During the northern fall season of MY 28, global dust storm occurred on Mars (Smith, 2009; Wolkenberg et al., 2017). Listowski et al. (2014) discussed possible contribution from a dust storm to the formation of the mesospheric CO_2 ice clouds. They calculated the sedimentation rates and the resulting dust size vertical distribution for the full dust size distribution with a radius grid ranging from 1 nm to 100 micrometers. The calculated dust number densities are small that their effect on the formation of observable clouds is negligible or cannot dominate during the full MY29 cloud season (Listowski et al., 2014). It does not support that the increase of CO_2 clouds detections in MY 29 is due to the global dust storm occurred in MY 28.* "

The statement in the abstract and conclusions are also modified accordingly.

2. Fig. 8 (Discussion on the non-detection of the secondary peak at 4.32-34 μm by PFS):

The reviewer #1 questioned the necessity of Fig. 8 and pointed out this figure was confusing. We agree on the comment by the reviewer #1. Thus, we remove Fig. 8 (i.e., analysis of OMEGA data by ourselves) presented in the previous manuscript, and simply discuss the reason why PFS could not detect the secondary peak at 4.32 μm with the hypothesis that the horizontal scale of the clouds with secondary peaks at 4.32 μm

are much smaller than the PFS-FOV, by referring to “redish points” of Määttänen et al. (2010)’s Figure 6. Of course, as the reviewer #2 pointed out previously, the Figure 6 of Määttänen et al. 2010 is just one example of tens of clouds that have large secondary peaks and that only one figure, where the high secondary peaks are very localized, cannot be used to generalize the statement to all clouds. We note that fact as well.

The revised text (Lines 409-414): "***Fig. 6*** *of Määttänen et al. (2010) showed that* CO_2 *ice clouds with large secondary peaks (the reddish points) are spatially localized: single or a few pixels. The FOV of PFS is about 500 times larger than that of single pixel of OMEGA. Even though we could not give a general statement since* ***Fig. 6*** *of Määttänen et al. (2010) is just one example of tens of clouds that have large secondary peaks observed by OMEGA, the horizontal scale of the clouds with secondary peak at 4.32-34 μm may be too small to be detected by PFS.*"

The sentence in the conclusion has been modified accordingly (Lines 437-438):
(Old) *"The other secondary peak observed by OMEGA (Montmessin et al., 2007) in the spectral range 4.32–4.34 μm cannot be detected by PFS."*

(New) *"The other secondary peak observed by OMEGA (Montmessin et al., 2007) in the spectral range 4.32–4.34 μm was not detected by PFS."*

In the following text, we explain how and where each point of the reviewer’s comments has been incorporated (our responses are shown in black and the reviewers’ comments are in green):

==========

Authors’ reply to comments by Reviewer#1:

==========

Line 38 (Abstract):

Moreover, CO2 ice clouds were preferentially detected at the observational LT range

between 15–16 h in MY 29…

I don’t think this sentence can be left alone in the abstract. It implicitly suggests that you also observed at the same local time during other years, at the same place.
You have observational biases as shown by your new Fig3a and this should be said.

For instance you can add:

“However, observational biases prevent from distinguishing local time dependency from interannual variation.”

==========

The reviewer is correct. We cannot distinguish local time dependency from inter-annual variation because of the observational biases. The sentence has been modified as the reviewer suggested (Lines 39-40). *“Moreover,* CO_2 *ice clouds were preferentially*

detected at the observational LT range between 15–16 h in MY 29. However, observational biases prevent from distinguishing local time dependency from inter-annual variation."

==========

Line 39-42 (Abstract):

In my opinion, and given the above, I don't think you can put so much emphasis on the global dust storm in the abstract. The dust storm of northern fall MY28 providing more nanometric nuclei during MY29 is a hypothesis that is not very well backed up by simple sedimentation time calculations I think and it could be mentioned in the discussion, but I don't think this fits in the abstract as such because the results do not speak in favor of dust storm bringing nuclei to the MY29 clouds between Ls=10° and Ls=30°. I think the initial abstract was fine.

"The global dust storm occurred at the northern fall in MY 28 could not be ruled out as a possible explanation for this." For what? This sentence is too vague, and it should be rephrased. Also "relatively long time" is too vague. How much time? If you think you need to keep this in the abstract I would rather formulate this way (see below) and after the last sentence I suggested above ("Observational biases (…) variation"): "Simple sedimentation time calculations suggest that the MY28 global dust storm may be responsible for an increase of cloud nuclei of a few nanometers in size, during early MY29." But I don't really agree with this, as explained in my comment about the dust storm part below.

==========

We have agreed with the reviewer. We discuss the hypothesis (a possible relationship between global dust storm and occurrences of the mesospheric CO_2 clouds) only in the main text. The sentences are removed in the abstract.

==========

Line 56-57 (Introduction):

The way it is written suggests Herr and Pimentel (1970) mention fluorescence, while it is not the case.

Suggestion:
The existence of mesospheric CO2 ice clouds on Mars was first suggested by the infrared spectra recorded by Mariner 6 and 7 (Herr and Pimentel,1970) although the low altitude of the detection (25 km) argues in favor of CO2 fluorescence (e.g Lellouch et al. , 2000).

Lellouch, E., T. Encrenaz, T. de Graauw, S. Erard, P. Morris, J. Crovisier, H. Feuchtgruber, T. Girard, and M. Burgdorf (2000), The 2.4– 45 mm spectrum of Mars observed with the infrared space observatory, Planet. Space Sci., 48, 1393–1405.

==========

The reviewer is correct, the way to refer Herr and Pimentel (1970) was not appropriate. The sentence has been corrected as the reviewer suggested (Lines 55-58): *"The*

existence of mesospheric CO_2 ice clouds on Mars was first suggested by the infrared spectra recorded by Mariner 6 and 7 (Herr and Pimentel, 1970) although the low altitude of the detection (25 km) argues in favor of CO_2 fluorescence (e.g Lellouch et al. , 2000).”

==========

Line 57-59 (Introduction):

The formation of the mesospheric CO2 ice clouds was really discussed from temperatures colder enough for CO2 condensation by the measurements of Pathfinder during its descent (Schofield et al., 1997), and submillimeter CO lines from the James Clerk Maxwell Telescope (JCMT) (Clancy and Sandor et al., 1998).

Sorry but the wording does not make sense. This should be rephrased. Simply say that Clancy and Sandor (1998) discussed the CO2 ice clouds formation based on Pathfinder measurements and submm observations etc.

==========

Based on the comment by the reviewer, the sentence has been modified (Lines 58-60): *“Clancy and Sandor et al. (1998) discussed the mesospheric CO_2 ice clouds formation based on vertical temperature profiles measured by Pathfinder during its descent (Schofield et al., 1997) and those by the James Clerk Maxwell Telescope.* ”

==========

Line 108-109 (Introduction):

What do you mean by “not well understood”?
I think this sentence is not needed, and does not sound right because then, just after, you describe the various constraints that exist on the crystal sizes.

You can have the paragraph describing the observational constraints on the crystal size. Then say that there are no constraints on the exact composition of the cloud crystals (pure CO2 ice or not), and on their shapes in the clouds.

“For the crystal composition and shape, there are no direct observations.” It is not true in terms of composition. We have information on the composition of the crystals since we know it is CO2 ice, we just don’t know whether it is mixed with other things (dust nuclei, water ice,...?), in other words wheter it is pure CO2 ice or not. Please rephrase.

==========

As the reviewer suggested, the first sentence in the paragraph “*However, the crystal size, composition, and shape of these mesospheric CO_2 ice clouds are not well understood.”* has been removed and the second sentence (i.e., first sentence in the revised manuscript) has been modified as follows *“the crystal size of the mesospheric CO_2 ice clouds was constrained by the spectroscopic observations. SPICAM-UV nighttime observations suggested that the effective radii of the CO_2 cloud crystals detected around 100 km are between 0.08 and 0.13 μm (Montmessin et al., 2006).”*. (Lines 109-112)

The final sentence in that paragraph has been also modified "*While understanding of the exact composition of the cloud crystals (pure CO_2 ice or not) and their shapes in the clouds are still poor because there are not direct observations.*". (Lines 120-121)

==========

Line 258 (Section 3):

I would say: "the resulting detection probability" to make clear that it is the detection probability mentioned above, and restrained to [20°S-20°N], etc.

==========

The text is modified as the reviewer suggested. (Line 259)

==========

Line 262 (Section 3):

Recall that it is because of the non-sun-synchronous orbit.

==========

The text is modified as the reviewer suggested. (Line 269)

==========

Line 264 (Section 3):

You should say that it is for the 20°S-20°N band, and for the Ls=10-30°. As such it is not clear if your statement is meant for all the clouds or only for the restricted region/season.

It seems to me that your observational bias shown in Figure 3a does not allow to write Line 264 as it is. I think you should clearly say that this applies to your dataset, and not to Mars in general.

==========

Based on the comment by the reviewer, the sentence is modified as follows (Lines 266-269): "*In the PFS dataset, the CO_2 clouds are most frequently observed around 15-16 LT and/or in MY29 for the 20°S-20°N band, and for the Ls=10-30°, however this conclusion cannot be generalized because of the significant inter-annual variations in observational coverage because of the non-Sun-synchronous orbit of MEx.* ".

==========

Line 264-266 (Section 3):

So what? It is not clear why those sentences are needed here. How are they related to what is stated before? "deeply" is not clear. "a preferred altitude" for what? Please be more precise in your statements. The two sentences are too vague.

If you really think you should cite this work here then something like the following could be said, for instance:

Gonzalez-Galindo et al. (2011) showed that the minima of temperature due to the thermal tides in their GCM occur at local times/altitudes where mesospheric clouds were observed. Thus, the local time formation for the cloud seems to be determined by the local time of the temperature minima of the thermal tides (as for the spatial distribution of the clouds). However, no detailed cloud simulation work investigated the full diurnal cycle of mesospheric CO2 cloud formation.

==========

Based on the comments by the reviewer, the sentence has been modified. (Lines 272-276)

==========

Lines 267-279 (Section 3): dust storm bit

In my opinion, this new bit about the dust storm does not fit here in this section which is about results on spatial, seasonal, and local time distribution. I think – if you keep it - this should go in the discussion part (section 5), because it presents a hypothesis trying to explain the variability observed in the PFS dataset for MY29.

Most of all, I am not convinced about the fact of saying that the storm brought the nuclei for clouds during year MY29 Ls=10-30°. You should be careful with your statements. Between Ls=310° and Ls=10° the following year there are approximately 100 sols (and so even more between Ls=310 and Ls=30, which is the end of the cloud detections during MY29). Note that 100 sols after the end of the global dust storm, the particle of size 4nm (if starting at 100 km altitude) ends just below 60 km altitude (according to your Figure B1). This is below many of the altitudes of mesospheric cloud detections. Note that all the clouds detected by OMEGA during MY29 between Ls=10 and Ls=30 were above 65 km altitude, and up to 85 km altitude! (Määttänen et al. 2010, Figure11b) so these calculations do not speak in favour of the cloud nuclei brought by the storm. This is also the conclusion of Listowski et al. (2014).

I understand you want to discuss the dust storm issue but then, you should be more careful with the wording because the numbers and calculations do not speak in favor of it as explained above… even for a 4nm particle!

Other comments on this part:
"we would like to note" not needed." Rephrase: "During the northern fall season of MY28, a global dust storm occurred…"

At Line 274-275, I don't think 60 sols is comparable to the gap between Ls=310° and Ls=10° the following year. Isn't it rather 100 sols? I think the way the sentence is written lead to think that there are 60 sols between those two Ls.

At Line 279. How do we know they can effectively act as nuclei? It is not enough to have nuclei, you need to have large enough supersaturation to activate them, especially for very small particles. Listowski et al. (2014), Figure 1, show that a 5nm particle needs saturation ratio S=5 to get activated, so 4nm could be around S=10. S=10 is about a cooling of 6K at 0.01 Pa (approx. 70-80km), which does not look unrealistic. In any

case, the fact of having a particle is not enough to make it an efficient cloud nuclei, it also depends on the saturation ratio needed to activate it, hence the ability of the atmosphere to cool enough below condensation point.

==========

We agree on the reviewer and shorten the discussion. Please see the main change "1" described above. Since the discussion is shortened, we keep it at this Section.

==========

Line 338 (Section 4):

This sentence needs to be reformulated:

Changing the altitude of the cloud, or the effective variance of the particle size distribution, do not impact the shape of the synthetic spectra (not shown).

==========

The sentence is reformulated as the reviewer suggested. (Lines 343-344)

==========

Line 379 (Section 5): "While there are no observations of the cloud particles shape…"

==========

The text has been corrected. (Line 384)

==========

Line 381 (Section 5): Need to add something at the end of the sentence, for clarity:

==========

A text has been added at the end of sentence for clarity: "*...and the nucleation of CO_2 ice crystals is most probably heterogeneous meaning that the crystal properties could be affected by dust grain inclusions*." (Lines 386-387)

==========

Line 385 (Section 5): Should not it be "CO2 ice crystal" rather than "CO2 ice cloud" ? It would make more sense. Remove the "although". Start new sentence: "The PFS spectra…"

==========

The texts have been corrected. (Line 391)

==========

Line 397 (Section 5): Use "characteristics" not "morphology".

==========

The texts have been corrected. (Line 403)

==========

Line 403 (Section 5): It is not clear to me what is to be seen in Fig. 5, related to what is being said. "See Fig. 5" is not enough to make the reader understand what is meant. Keep and explain, or remove "(see Fig. 5)".

==========

The word "(see Fig. 5)" has been removed. (Line 409)

==========

Line 403-409 (Section 5): about Figure 8

What do you mean we "visualize" the OMEGA spectra ? As far as I understand it is new data that is brought here? There should be a few words/sentences explaining that you are using new data here! "We visualize…" is not enough and it comes out of the blue. I don't understand Figure 8. It is not because the radiance at 4.32um is smaller than the one at 4.26um, that there is no secondary peak at 4.32um! I don't understand how this shows that "having the secondary peak at 4.32um is rare". There should be much more explanations. To me, it is not clear at all. Also, I don't understand why you need to show Figure 8. It does not bring much, and is not needed. Also it is not because the 4.32um peak would be "rare" that it explains why PFS cannot detect it! Or if it does, there should be more explanations. As such, this is very confusing.

In the previous version of the manuscript, the authors were speaking about "spatially localized" features, referring to "redish points" of Määttänen et al. (2010)'s Figure 6. It was said (I quote):

Because the sizes of the clouds with secondary peaks at 4.32–4.34 μm are much smaller than the FOV, PFS most likely cannot detect these clouds. In fact, Fig. 6 of Määttänen et al. (2010) suggests that CO2 ice clouds with large secondary peaks are spatially localized (see the reddish points in Fig. 6 of Määttänen et al. (2010)).

To me the idea was to try and compare the actual spatial extension of those reddish points (using OMEGA spatial resolution and looking at the example of Fig6 in Määttänen et al. 2010 – I think there is no need to go and use the OMEGA spectra), and compare to PFS FOV and spatial resolution, perhaps that would help to discuss the fact you are not observing the peak at 4.32 um. Some quantitative comparisons of spatial resolution of the instruments, spatial extension of those "reddish points", and comparisons to the FOV of instruments would help discuss this more consistently I think. In any case it is not clear why Figure 8 says something about the fact PFS does not detect 4.32um feature, or why it says that 4.32um is rare.

==========

We agree on the comment by the reviewer. Figure 8 is removed. In the revised manuscript, as the reviewer suggested, we simply discuss the hypothesis that the horizontal scale of the clouds with secondary peaks at 4.32 μm are much smaller than the PFS-FOV, by referring to "redish points" of Määttänen et al. (2010)'s Figure 6. Please see the main change "2" described above.

==========

Line 443 (Section 6): Explicit DDA for the conclusion

Line 444 (Section 6): Was used by Isenor et al. (3013) for what? Be more explicit in the conclusion.

Line 444-445 (Section 6): "DDA… is able to…" is not correct. It should be rephrased:

DDA… would allow to model IR spectra … to be compared to PFS spectra.

Line 445-446 (Section 6): "will provide": is this planned? Or do you rather mean "can provide"

Line 446 (Section 6): "(including the reason for the secondary peak)": what does this mean exactly? I think it should be removed for clarity.

Line 447 (Section 6): "morphology" is not appropriate. What about "characteristics" or rather "microphysical characteristics" or just "microphysics"?

==========

Based on the comments by the reviewer, the sentences are modified as follows: "*The discrete dipole approximation (DDA), which is widely used for non-spherical particles modeling in astronomy and planetary science and was used in the simulation demonstrated by Isenor et al. (2013), would allow us to model IR spectra of non-spherical crystals to be compared with the PFS spectra. Detailed comparison between the measured PFS spectra and those modeled by the DDA can provide new insight on the microphysical characteristics of these mesospheric CO_2 ice clouds.*" (Lines 449-454).

==========

Line 694 (Appendix B): I think it should be said "eddy diffusion".

Line 714 (Appendix B): What is the upper dust maximum? Please define it.

Line 736 (Appendix B): to fall down to altitude of around à to fall to an altitude of around

Line 738 (Appendix B): "Time of falling down". Rather say and define a "sedimentation time".

Line 738-739 (Appendix B): the formula for a constant velocity (1) and for free fall case (2) à What are they? You should present them, and explain what it means.

Figures B1 and B2 (Appendix B): Both times are very close, you don't need to show both. You can work with one time only. Also, I don't think you need to show the plot of the fall speed. The Figure of the sedimentation time is enough (and just one of both "cases"). Also, the title of the plot is always "sedimentation velocity" and it should be removed or corrected. In the end you could have only One Figure/plot, and not four plots.

==========

Thank you very much for the comments for Appendix B. As we explained in the "Main change 1", we decide to remove this Appendix.

==========

Authors' reply to comments by Reviewer#2:

==========

The only bigger comment I have is related to the predominance of observations around 15-16 LT in MY29, and the effect of the MY28 dust storm on the occurrence of CO2 clouds in MY29. Unfortunately, I still don't think the authors have a solid case. They claim that, as according to their calculations particles of 4 nm can stay above 60 km during more than 60 sols, such particles lofted to the mesosphere by the MY28 dust storm could act as condensation nuclei for the MY29 clouds. They also still state that "Although the MEx observations could not distinguish between local time dependence and inter-annual variation, our results and the previous OMEGA analysis suggest that the mesospheric CO2 ice clouds preferentially formed around 15–16 h and/or in MY 29." Despite their response to my previous comment on this, I still think they should change their conclusion into "In the PFS dataset, the CO2 clouds are most frequently observed around 15-16 LT and/or in MY29, but this conclusion cannot be generalized because of the significant interannual variations in observational coverage." I'm giving some justifications in the following.

First, Listowski et al. (2014), who the authors cite, calculated the sedimentation rates and the resulting dust size vertical distribution for the full dust size distribution with a radius grid ranging from 1 nm to 100 micrometers, so they do include very small particles in their calculation. However, the dust number densities are so small that their effect on the formation of observable clouds will be negligible and/or cannot dominate during the full MY29 cloud season. In addition to this, the supersaturations required to activate these very small particles as condensation nuclei are very large, making the cloud formation an even more difficult process.

Also, the Upper Dust Maximum (UDM) reported by Guzewich et al. (2013) is suggested in the appendix of this manuscript as a justification for saying that dust coming from a global dust storm can be lifted to high altitudes and remain there for a long time. However, Guzewich et al. (2013) stated that the UDM showed strong diurnal variations and was not related to dust storms. Thus, it cannot be used here as a basis for high dust lifted by dust storms. In addition, Kleinboehl et al. (2015) showed that MCS observations did not detect the UDM even though MCS has the required sensitivity, and that they do not support the conclusions of Guzewich et al. (2013). They mentioned that a systematic radiometric error of TES reported by Pankine (2015) might explain why the UDM appeared in the retrievals of Guzewich et al. (2013). So according to the MCS observations of Kleinboehl et al. (2015), the UDM does not exist.

Considering the above points and that the fall velocities are easy to calculate, the discussion could be shortened significantly. There is no need for the two different equations of Appendix B nor the two different figures B1 and B2. If the authors wish to state something on the effect of a dust storm on the cloud formation, they would also need to estimate the number densities and the size distribution of the dust particles that can be lofted up to 100 km and model then their sedimentation to arrive at a realistic number density distribution of nanometer-size particles, and then show that these particles are enough to create observable clouds even 60 degrees in Ls later.

Second, looking at the latitude-solar longitude-local time coverage of PFS on different Martian Years, it is not possible to state anything about the preferential (or not)

formation of mesospheric CO2 clouds at certain local times or Martian Years. Very simply, if there are no observations in the afternoon during the clouds seasons of the other Martian Years, one cannot say that the clouds form preferentially in the afternoon. For any interannual variations the conclusion is the same: if the coverage is insufficient, the different years cannot be compared. The only case where this maybe could be done is between MY29 and MY30, since in the latter the latitude-Ls coverage during the cloud season is quite good with local times in the early afternoon and late morning. In MY30 PFS actually observes quite a lot of morning clouds!

In addition, there are plenty of OMEGA observations of CO2 clouds in the beginning of MY27, although in the morning hours. PFS does not have coverage in that season in MY27. We simply cannot know, even with the combined coverage of PFS and OMEGA, if the Mars Years 27 and 29, and maybe MY30 as well, were somehow more favorable for mesospheric CO2 cloud formation, or not, and if cloud formation is favored in the afternoon or not.

==========

We agree on the reviewer and shorten the discussion. Please see the main change "1" described above.

Moreover, the statement in the previous manuscript "*Although the MEx observations could not distinguish between local time dependence and inter-annual variation, our results and the previous OMEGA analysis suggest that the mesospheric CO_2 ice clouds preferentially formed around 15–16 h and/or in MY 29.*"

has been replaced by

"*In the PFS dataset, the CO_2 clouds are most frequently observed around 15-16 LT and/or in MY29 for the 20°S-20°N band, and for the Ls=10-30°, however this conclusion cannot be generalized because of the significant inter-annual variations in observational coverage because of the non-Sun-synchronous orbit of MEx.*"

as the reviewer suggested (Lines 266-269).

==========

Line 51: "deposition" should be "condensation" (Condensation is a correct term for the vapor-ice phase transition. Deposition is generally understood as something deposited on a surface, which might create confusion in this context, even though technically the phase transition on Mars is deposition mode nucleation where the vapor deposits directly as ice onto the surface of ice nuclei.)

==========

The text has been corrected. (Line 53)

==========

Line 57: "colder" should be "cold"

==========

The text has been removed.

==========

Line 82: “was” should be “were”

==========

The text has been corrected. (Line 83)

==========

Lines 188-199: “For the crystal composition and shape, there are no direct observations.” There are for the H2O/CO2 composition. I guess the authors mean that no observation allows for detection of the possible dust grain inclusions in the crystals?

==========

Yes, the reviewer is correct and it was misleading. We have modified the text as follows: “*While understanding of the exact composition of the cloud crystals (pure CO_2 ice or not), and their shapes in the clouds are still poor because there are not direct observations.* ” (Lines 120-121).

==========

Line 273 and appendix B: I think the statement should be softened here. The mentioned 60 sols correspond to about 32 degrees in solar longitude. The difference, as stated by the authors, between the end of the dust storm (Ls=310) and the beginning of the cloud season (Ls=10) is 60 degrees in Ls, which is twice the stated 60-sol period. The 4 nm particles would have fallen well below 60 km by the time of the cloud season start. In addition, as mentioned before, it is not only the particle size that matters, but also the number density that will in the end define the opacity, and thus the detectability, of the clouds. The number density of these 4nm particles will be so small that, even if activated, they will not be able to for optically thick enough clouds.

==========

As described above, the discussion is shortened and softened. Moreover, the Appendix B has been removed.

==========

Line 309: “gases” should be “gas”

==========

The text has been corrected. (Line 315)

==========

Line 380: “…and the nucleation of CO2 ice crystals is most probably heterogeneous…”; add “meaning that the crystal properties could be affected by dust grain inclusions”

==========

The suggested statement has been added. (Line 387)

==========

Line 396: “morphology” should rather be “properties”

==========

The text has been corrected, however, replaced by “*characteristics*” as the other reviewer suggested. (Line 403)

==========

Conclusion, lines 422-425: Please see my previous comments on this topic. It should also be kept in mind that even if small dust particles can remain lofted in the mesosphere, their number density is extremely small, which might not be enough for attaining observable cloud optical thicknesses.

==========

Based on the comments by the reviewer, the statement in the conclusion has been updated as follows: "*Moreover, mesospheric CO_2 ice clouds were found preferentially in the spectra taken in the late afternoon (15–16 h) in MY 29 even though this cannot be generalized because of the observational biases.*" (Lines 427-429).

==========

Figure 3: I think the statistics of panel c should be calculated for exactly the same data as in panel b, since otherwise it might be misleading if the reader does not read carefully the figure legend. The legend itself is slightly misleading as it is, since it is not clear if the data selection is applied in panels b and c, or only in c. If the panel c will not be changed, please add "In panel c," in the beginning of the sentence "Only detections within…" So: "In panel c, only detections within the latitudes …, longitudes …, and season of … were used for these statistics to exclude observational biases."

==========

In order to avoid the misleading of the figures, the legend "statistics for the detections at 20°S–20°N, −110°E to +30°E, *Ls* = 10–30°" has been added in Fig. C. Moreover, The caption for Fig. C has been modified as the reviewer suggested.

Thank you for the attention and constructive criticism that has resulted, we believe, in a much better paper.

Sincerely Yours,
Authors.

Highlights

We investigated Martian mesospheric CO_2 ice clouds using MEx/PFS observations.

The spatial and seasonal distributions are consistent with previous reports.

The main CO_2 scattering peak was found between 4.240 and 4.265 μm.

We report the first detection of an occasional secondary peak at 4.28 μm.

The spectral features cannot be simulated using Mie theory.

Mesospheric CO_2 ice clouds on Mars observed by Planetary Fourier Spectrometer onboard Mars Express

S. Aoki[a,b,c,d,*], Y. Sato[c], M. Giuranna[d], P. Wolkenberg[d,e], T. M. Sato[f], H. Nakagawa[c], and Y. Kasaba[c]

[a] Belgian Institute for Space Aeronomy (IASB-BIRA), Ringlaan-3-Avenue Circulaire, Uccle 1180, Brussels, Belgium.
[b] Fonds National de la Recherche Scientifique (FNRS), 5 rue d'Egmont, B-1000 Brussels, Belgium
[c] Department of Geophysics, Graduate school of Science, Tohoku University, Aramaki Aza Aoba
[d] Istituto di Astrofisica e Planetologia Spaziali (IAPS), Istituto Nazionale di Astrofisica (INAF), Via del Fosso del Cavaliere 100, 00133 Rome, Italy.
6-3, Aoba, Sendai, Miyagi 980-8578, Japan.
[e] Centrum Badań Kosmicznych Polskiej Akademii Nauk (CBK-PAN), ul. Bartycka 18A, 00-716 Warszawa, Poland
[f] Institute of Space and Astronautical Science (ISAS), Japan Aerospace Exploration Agency (JAXA), 3-1-1, Yoshinodai, Chuo-ku, Sagamihara, Kanagawa 252-5210, Japan.

Mars; Mars, atmosphere; Mars, climate; Infrared observations; Spectroscopy

Corresponding author:
Shohei Aoki
Belgian institute for Space Aeronomy (IASB-BIRA), Ringlaan-3-Avenue Circulaire, Uccle 1180, Brussels, Belgium.
E-mail: shohei.aoki@aeronomie.be

Abstract

We have investigated mesospheric CO_2 ice clouds on Mars through analysis of near-infrared spectra acquired by Planetary Fourier Spectrometer (PFS) onboard the Mars Express (MEx) from MY 27 to MY 32. With the highest spectral resolution achieved thus far in the relevant spectral range among remote-sensing experiments orbiting Mars, PFS enables precise identification of the scattering peak of CO_2 ice at the bottom of the 4.3 μm CO_2 band. A total of 111 occurrences of CO_2 ice cloud features have been detected over the period investigated. Data from the OMEGA imaging spectrometer onboard MEx confirm all of PFS detections from times when OMEGA

operated simultaneously with PFS. The spatial and seasonal distributions of the CO_2 ice clouds detected by PFS are consistent with previous observations by other instruments. We find CO_2 ice clouds between *Ls* = 0° and 140° in distinct longitudinal corridors around the equatorial region (± 20°N). Moreover, CO_2 ice clouds were preferentially detected at the observational LT range between 15–16 h in MY 29. However, observational biases prevent from distinguishing local time dependency from inter-annual variation. ~~The global dust storm occurred at the northern fall in MY 28 could not be ruled out as a possible explanation for this. Our calculation shows that small dust particles (of the order of a few nm) can remain suspended in the mesosphere for a relatively long time and act as condensation nuclei of the CO_2 ice clouds.~~ PFS also enables us to investigate the shape of mesospheric CO_2 ice cloud spectral features in detail. In all cases, peaks were found between 4.240 and 4.265 μm. Relatively small secondary peaks were occasionally observed around 4.28 μm (8 occurrences). These spectral features cannot be reproduced using our radiative transfer model, which may be because the available CO_2 ice refractive indices are inappropriate for the mesospheric temperatures of Mars, or because of the assumption in our model that the CO_2 ice crystals are spherical and composed by pure CO_2 ice.

1. Introduction

One of the peculiar phenomena of the Martian climate is the existence of carbon dioxide (CO_2) ice clouds. These clouds are formed by ~~deposition~~ condensation of the major constituent of the Martian atmosphere, CO_2. Recent observations have revealed the presence of the CO_2 ice clouds at remarkably high altitudes (above 40 km; mesosphere). The existence of mesospheric CO_2 ice clouds on Mars was first suggested by the infrared spectra recorded by Mariner 6 and 7 (Herr and Pimentel, 1970) although the low altitude of the detection (25 km) argues in favor of CO_2 fluorescence (e.g Lellouch et al., 2000). Clancy and Sandor et al. (1998) discussed the mesospheric CO_2 ice clouds formation based on vertical temperature profiles measured by Pathfinder during its descent (Schofield et al., 1997) and those by the James Clerk Maxwell Telescope. Subsequently, Montmessin et al. (2006) detected several mesospheric detached layers at an altitude of around 100 km at [32°S, −178°E, *Ls* = 134°], [36°S, 134°E, *Ls* = 135°], [15°S, 15°E, *Ls* = 137°], and [15°S, −83°E, *Ls* = 137°] from the nighttime measurements by SPectroscopy for the Investigation of the Characteristics of the Atmosphere of Mars (SPICAM) ultraviolet (UV) channel onboard Mars Express (MEx). These detached layers were attributed to the presence of CO_2 ice crystals because of the simultaneous detection of a supersaturated cold pocket just above the aerosol layer.

A global view of these mesospheric CO_2 ice clouds has been provided by Observatoire pour la Minéralogie l'Eau les Glaces et l'Activité (OMEGA) onboard MEx and the Compact

Reconnaissance Imaging Spectrometer for Mars (CRISM) onboard Mars Reconnaissance Orbiter (MRO) daytime observations (Montmessin et al., 2007; Määttänen et al., 2010; Vincendon et al., 2011). From the OMEGA data, mesospheric CO_2 ice clouds were identified through a more straightforward approach. A distinct peak was detected at the bottom of the 4.3-μm CO_2 gas band, caused by scattering of CO_2 ice cloud crystals in the mesosphere (Montmessin et al., 2007). The fundamental ν_3 band of CO_2 ice is possibly the strongest known infrared band for a molecule (Warren, 1986), and the combination of the dramatic increase of the imaginary part of the CO_2 ice index and large fluctuation of the real part produces a sharp peak around 4.26 μm. From the OMEGA data analysis, a total of 60 occurrences were identified during the period from MY 27 to 29 (Määttänen et al., 2010) and 13 occurrences in MY 30 (Vincendon et al., 2011). Additionally, CRISM daytime measurements detected the mesospheric CO_2 ice clouds via indirect spectral identification. Although CRISM is a similar instrument to OMEGA, it does not observe the distinctive scattering peak at the bottom of the 4.3 μm CO_2 band because of its limited spectral range (0.362–3.92 μm). Instead, cloud features were identified from the CRISM RGB composite images (based on wavelengths of 0.592, 0.533, and 0.492 μm), and CO_2 ice clouds ~~was~~ were distinguished from H_2O ice based on the CRISM IR spectra. From the CRISM observations during the period from MY 29 to MY 30, 54 occurrences in total were found (Vincendon et al., 2011). These detections by OMEGA and CRISM are mainly within a distinct longitudinal corridor (−120°E to +30°E) around the equatorial region (20°S to 20°N) during the aphelion season (Ls = 330–150°), with the exception of two detections by OMEGA at mid-latitudes at [49.1°S, −138.3°E, Ls = 54.2°] and [46.6°N, −74.7°E, Ls = 246.3°], one detection by CRISM around 155°E, and one by OMEGA around 120°E.

The formation mechanism of the mesospheric CO_2 ice clouds has been discussed based on the observed spatial and seasonal distributions. Clancy and Sandor (1998) first suggested a scenario whereby the clouds form in supersaturated pockets of air created by the interference of thermal tides and gravity waves. This scenario has been demonstrated by theoretical studies. González-Galindo et al. (2011) showed using a Mars Global Circulation Model that the observed mesospheric CO_2 ice clouds can be found in places where temperature minima are reached in the atmosphere due to the propagation of thermal tides. This study showed that observations were significantly correlated with the seasonal and spatial distributions of these minima caused by the propagation of the large-scale waves, even though the temperature remained just above the condensation threshold. Subsequently, Spiga et al. (2012) showed using a mesoscale model that the locations where clouds are observed are places where gravity waves are not filtered by Martian atmospheric dynamics and can propagate upward into the mesosphere. This study supported the

inference that smaller-scale waves allow the creation of supersaturated pockets in the temperature minima created by the thermal tides. Finally, Listowski et al. (2014) demonstrated that temperature profiles that combine the effects of thermal tides and gravity waves in a one-dimensional microphysical bin model enable simulation of mesospheric CO_2 ice clouds that are consistent with observations.

~~However, the crystal size, composition, and shape of these mesospheric CO_2 ice clouds are not well understood.~~ The crystal size of the mesospheric CO_2 ice clouds was constrained by the spectroscopic observations. SPICAM-UV nighttime observations suggested that the effective radii of the CO_2 cloud crystals detected around 100 km are between 0.08 and 0.13 μm (Montmessin et al., 2006). In contrast, larger crystal sizes were estimated from the daytime observations at lower altitudes (~60-80 km) by OMEGA and CRISM. The OMEGA analysis showed that crystal radii are within 1–3 μm, and that their optical depths are between 0.01 and 0.6 at λ = 1 μm (Määttänen et al., 2010); the CRISM analysis showed that crystal radii are within 0.5–2 μm and, that their optical depths are lower than 0.3 at λ = 0.5 μm (Vincendon et al., 2011). These estimates were calculated by comparing the measurements and simulations based on the Mie theory (with spherical particle shape assumed). Note that in the OMEGA data analysis, the peak at 4.3 μm was not used directly; the crystal size was derived from ratios between the radiances inside and outside shadows. While understanding of the exact composition of the cloud crystals (pure CO_2 ice or not) and their shapes in the clouds are still poor because there are not direct observations.

In this study, we have investigated these mesospheric CO_2 clouds using the nadir near-infrared spectra of the Planetary Fourier Spectrometer (PFS) onboard MEx. To date, PFS has the highest spectral resolution in the 4.3 μm CO_2 band. Using this unique dataset, a detailed study has been conducted on the spectral position, shape, and intensity of the CO_2 ice cloud scattering peak around 4.3 μm. The high-spectral-resolution observations of PFS provide not only a new dataset to compare with previous observations but also new insights into the optical properties of the mesospheric CO_2 ice clouds (such as crystal size, composition, and shape). The details of the PFS data analysis are described in Section 2. The observational results are presented in Section 3. A comparison between the spectra measured by PFS and synthetic spectra from a radiative transfer model is provided in Section 4, and the results are discussed in Section 5. Finally, concluding remarks are provided in Section 6.

2. PFS Data Analysis

2.1. Planetary Fourier Spectrometer (PFS)

PFS is a Fourier transform spectrometer onboard the MEx orbiter optimized for atmospheric

studies (Formisano et al., 2005). It has two spectral channels: the Short Wavelength Channel (SWC, 2000–8600 cm^{-1}) and the Long Wavelength Channel (LWC, 250–1700 cm^{-1}). The fields of view are 1.6° for the SWC and 2.8° for the LWC. Both channels have a spectral sampling step of 1.0 cm^{-1} and a spectral resolution of 1.3 cm^{-1}. The spectral and radiometric calibration procedure for both channels has been discussed in detail by Giuranna et al. (2005a, b). An advantage of PFS is its wide spectral coverage coupled with its relatively high spectral resolution. In about six Martian years, PFS has collected more than 2,500,000 spectra for each channel. With full spatial coverage every year, PFS has been sounding the Martian atmosphere at different local times and seasons, which enables investigation of the diurnal, seasonal, and inter-annual variability of several atmospheric constituents and optical parameters of aerosols.

2.2. Searching for mesospheric CO_2 ice cloud features with PFS

In this study, we have analyzed PFS spectra collected over a period of about six Martian years, from July 2004 to March 2015 (MEx Orbit #634–14454), which corresponds to the beginning of MY 27 and the end of MY 32, respectively. To detect mesospheric CO_2 ice clouds, the scattering peak of CO_2 ice at the bottom of the 4.3 μm CO_2 band in the SWC spectra was searched. Because the lines of this strong CO_2 band are saturated, no solar reflection signal is expected between 4.2 and 4.5 μm, except in the following three cases (Montmessin et al., 2007): (1) solar reflection from high topographic regions (i.e., partial desaturation of the CO_2 band), (2) non-local thermodynamic equilibrium (non-LTE) emission of CO_2 and CO, and (3) solar reflection by high-altitude aerosols, such as mesospheric CO_2 ice clouds. In the first case, an emission-like feature gradually appears around 4.38 μm with increasing surface altitude because of the weaker amplitudes of the CO_2 absorption lines at that wavelength (Rothman et al., 2013). The second case typically occurs in PFS limb observations, when non-LTE spectral features appear within a wide spectral range between 4.15 and 4.5 μm (Formisano et al., 2006). As we are only interested in the mesospheric CO_2 ice clouds, we carefully selected nadir-only observations with emission angles lower than 30° and relative to surface altitudes lower than 8 km. These criteria exclude limb observations and guarantee saturation of the 4.3-μm band.

We built an algorithm to detect mesospheric CO_2 ice clouds from the PFS spectra. In this algorithm, two parameters (d_1 and d_2) were introduced:

$$d_1 = \max\left\{I_{PFS}(\lambda) - I_0(\lambda)\right\}_{\lambda=4.22-4.35\mu m},$$

168 $$d_2 = \frac{1}{d} \sum_{\lambda=4.22\,\mu m}^{4.35\,\mu m} \left(\frac{I_{PFS}(\lambda) - F(\lambda)}{\sigma(\lambda)}\right)^2 ,$$

169 where I_{PFS} is the PFS radiance smoothed with five spectral points (to improve the signal to noise
170 ratio); I_0 is the background radiance between 4.22 and 4.35 μm, which was estimated by linear
171 regression from the two spectral ranges at 4.20–4.22 and 4.35–4.37 μm; F is the best-fit quadratic
172 function with the smoothed PFS radiance for wavelengths within the range of 4.22–4.35 μm; d is
173 the degree of freedom in the fitting (i.e., the number of spectral points N in the wavelength range
174 4.22–4.35 μm minus 2); and σ is the noise equivalent radiance (NER) of PFS. The first parameter,
175 d_1, is the maximum radiance at wavelengths between 4.22 and 4.35 μm, which is used to identify
176 the scattering peak of CO_2 ice at the bottom of the 4.3 μm CO_2 band. To derive this parameter, the
177 deviation of the smoothed PFS spectra (I_{PFS}) from the background radiance (I_0) is calculated for the
178 spectral range 4.22–4.35 μm. The second parameter, d_2, is a reduced chi-square value of the
179 quadratic polynomial fit to I_{PFS} at wavelengths between 4.22 and 4.35 μm, which is used to
180 distinguish the data with spectral features of CO_2 ice clouds from those with relatively large noise.
181 To derive this parameter, a quadratic function was applied to the smoothed PFS spectra (I_{PFS}) for
182 wavelengths between 4.22 and 4.35 μm. Spectra were selected as possible candidates for showing
183 CO_2 ice cloud features if their d_1 value was three time larger than their NER value (~0.013
184 erg/sr/cm^2/cm^{-1}) and if their d_2 value was larger than 1.2. Then, possible candidates for CO_2 cloud
185 features were screened visually to check if they are associated with high topography or
186 instrumental problems. This algorithm and the threshold values for d_1 and d_2 were obtained from
187 experimental tests using spectra from orbit #5267. During that orbit, both PFS and OMEGA
188 operated simultaneously (both onboard MEx), and OMEGA detected extensive mesospheric CO_2
189 ice clouds (Määttänen et al., 2010).
190
191 **Figure 1a** shows a typical dayside spectrum of PFS in the spectral range between 4.0 and 4.5
192 μm, which has no CO_2 ice cloud features ($d_1 < 0.039$, $d_2 < 1.2$). About 96.93% of the PFS spectra
193 in the selected dataset do not have any particular features at the bottom of the 4.3 μm CO_2 band
194 (i.e., $d_1 < 0.039$, $d_2 < 1.2$), such as the spectrum shown in **Fig. 1a**. In contrast, the two spectra
195 shown in **Figs. 1b** and **1c** indicate CO_2 ice cloud features, which are identified by the algorithm
196 (i.e., $d_1 > 0.039$, $d_2 > 1.2$). In total, 111 occurrences of such mesospheric CO_2 ice cloud features
197 were identified, which constitutes about 0.01% of the spectra in the selected dataset. Note that one
198 of the two examples has a secondary peak around 4.28 μm (**Fig. 1c**), although these two spectra
199 were obtained at almost the same region and time. This secondary peak has not previously been

reported because the spectral resolution of OMEGA cannot resolve this feature. The small secondary peak was observed in about eight occurrences in total. The rest of the PFS spectra (i.e., 3.06% of the spectra in the selected dataset) have high maximum radiance ($d_1 > 0.039$) but low chi-square values ($d_2 < 1.2$) because of relatively large noise. **Fig. 1d** shows an example of these cases. As shown in this figure, the relatively large noise provides a large d_1 value, although a distinct scattering peak is not visible. To exclude such cases, the second parameter, d_2, is introduced in the algorithm.

Table 1 provides a list of the mesospheric CO_2 ice clouds detected from the selected PFS data using the algorithm. We compared these detections with those reported by OMEGA measurements during MY 27–30 for validation (Tables 3 and 4 in Määttänen et al., 2010; Table 3 in Vincendon et al., 2011). During a period of simultaneous operation between OMEGA and PFS in MY 27-30, 100% of the PFS detections were also confirmed by the OMEGA data (51 cases), which demonstrates that this algorithm is robust enough to detect these cloud features. However, the algorithm is not optimized for weak signals, such as optically thin clouds or small clouds (relative to the PFS-FOV). **Fig. 1e** shows one of the spectra without CO_2 ice cloud features classified by the algorithm ($d_1 < 0.039$, $d_2 < 1.2$) but with possible CO_2 ice cloud features around 4.25 μm. Although developing a robust algorithm to detect such weak signal is not a trivial task, such occurrences can be detected by eye. After visual inspection of the entire PFS dataset, we identified an additional 175 occurrences of CO_2 ice clouds, as described and listed in the **Appendix A**.

3. Spatial, seasonal, and local time distributions

Figure 2 shows the spatial and seasonal distributions of the mesospheric CO_2 ice clouds detected in PFS spectra with the algorithm described in Section 2. CO_2 ice clouds were detected within a longitudinal range of −100.6°E to +23.2°E (109 cases) and around +161°E (two cases) over equatorial latitudes from 15.6°S to 21.5°N, and in the seasonal range between Ls = 8.9° and 134.6°. Most of these clouds occurred between Ls = 10° and 30° (87 cases). The locations and season in which mesospheric CO_2 ice clouds were detected are consistent with previous spectroscopic observations by OMEGA and CRISM (Montmessin et al., 2007; Määttänen et al., 2010; Vincendon et al., 2011). In particular, the distributions shown by the PFS data are similar to those observed by CRISM (Vincendon et al., 2011). No CO_2 ice clouds were detected from the PFS data at mid-latitudes, where both SPICAM and OMEGA have detected such clouds. SPICAM observed two occurrences of such mid-latitudes clouds around [32°S, −178°E] (LT = 1:00) and [36°S, +134°E] (LT = 24:00) at Ls = 134–135° (Montmessin et al., 2006). It is reasonable to infer that PFS could not detect such clouds because these were detected by SPICAM in nighttime,

whereas PFS measurements are performed in daytime. Moreover, the effective crystal radii of the CO_2 ice clouds detected by SPICAM were estimated to be between 0.08 and 0.13 μm (Montmessin et al., 2006), and our radiative transfer calculations suggest that no scattering peak forms at the bottom of the 4.3-μm band with such small crystals (see Section 4 and **Fig. 5**). In contrast, OMEGA identified two mid-latitude clouds based on the scattering peak of CO_2 ice at 4.3 μm from daytime observations around [46.6°N, −74.7°E] at Ls = 246.4° (LT = 14.1) and [49.1°S, −138.3°E] at Ls = 54.2° (LT = 7.9) (Määttänen et al., 2010). Unfortunately, PFS did not conduct simultaneous observations with OMEGA for these detected mid-latitudes clouds. As shown in **Fig. 6** of Määttänen et al. (2010), the horizontal scale of the mid-latitude clouds is about 35 km. In principle, such clouds can be detected even with the relatively large FOV of PFS (about 7 km at the pericenter). Note that even by eye, mid-latitudes CO_2 clouds could not be found in the PFS dataset (see **Appendix A**). The PFS and OMEGA results suggest that the presence of CO_2 clouds at mid-latitudes is an unusual event.

As shown in **Fig. 3a**, PFS measurements have different local times (LT) for each MY because of the non-Sun-synchronous orbit of MEx. **Fig. 3b** shows the number of the mesospheric CO_2 ice cloud detections of PFS with the corresponding observational LT and MY. We detected mesospheric CO_2 ice clouds at local times between 8.3 and 17.9 h, except during 10–11 h, with a maximum at 15–16 h. The low radiance before 8 h and after 18 h did not allow detection of the clouds. The previous OMEGA study detected clouds between 7.9 and 17.3 h except during 12–13 h (Määttänen et al., 2010). To investigate the LT dependence of mesospheric CO_2 ice clouds, the detection probability for a given LT, which is equal to the number of mesospheric CO_2 ice cloud detections at that LT divided by the total number of measurements at that LT, was calculated at 1-h intervals for local times between 8 and 18 h. The PFS observations within the latitudinal range of 20°S to 20°N, the longitudinal range of −110°E to +30°E, and the solar longitudinal range of 10° to 30° were used for this calculation to reduce the effects of spatial and seasonal dependence of the observational local time. **Fig. 3c** shows the resulting detection probability of mesospheric CO_2 ice clouds. As shown in this figure, we have found that mesospheric CO_2 ice clouds are preferentially detected in spectra taken in the late afternoon (15–16 h), which were all measured in MY 29. Määttänen et al. (2010) also reported that numerous clouds were detected around 15–16 h in the OMEGA data collected in MY 29. ~~Although the MEx observations could not distinguish between local time dependence and inter-annual variation, our results and the previous OMEGA analysis suggest that the mesospheric CO_2 ice clouds preferentially formed around 15–16 h and/or in MY 29.~~ In the PFS dataset, the CO_2 clouds are most frequently observed around 15-16 LT and/or in MY29 for the 20°S-20°N band, and for the Ls=10-30°, however this conclusion cannot be

generalized because of the significant inter-annual variations in observational coverage because of the non-Sun-synchronous orbit of MEx.

~~So far, no modeling study has deeply investigated the diurnal cycle of the CO_2 clouds, however, Gonzalez-Galindo et al. (2011) suggested that there is a preferred altitude depending on local time.~~ Gonzalez-Galindo et al. (2011) showed that the minima of temperature due to the thermal tides in their GCM occur at local times/altitudes where mesospheric clouds were observed. Thus, the local time formation for the cloud seems to be determined by the local time of the temperature minima of the thermal tides (as for the spatial distribution of the clouds). However, no detailed cloud simulation work investigated the full diurnal cycle of mesospheric CO_2 cloud formation.

During the northern fall season of MY 28, global dust storm occurred on Mars (Smith, 2009; Wolkenberg et al., 2017). Listowski et al. (2014) discussed possible contribution from a dust storm to the formation of the mesospheric CO_2 ice clouds. They calculated the sedimentation rates and the resulting dust size vertical distribution for the full dust size distribution with a radius grid ranging from 1 nm to 100 micrometers. The calculated dust number densities are small that their effect on the formation of observable clouds is negligible or cannot dominate during the full MY29 cloud season (Listowski et al., 2014). It does not support that the increase of CO_2 clouds detections in MY 29 is due to the global dust storm occurred in MY 28.

We can partially constrain the altitude of the detected CO_2 ice clouds based on temperature profiles retrieved from PFS thermal-infrared data which allow retrievals of the atmospheric temperatures from 0 to 50 km from the 15-μm CO_2 band (e.g., Grassi et al., 2005a). The uncertainty of the retrieved vertical temperature profile is less than 2 K at 5–20 km and increases to 7 K at 50 km, and nadir view of the 15-μm CO_2 band is not sensitive temperature above 50 km (Grassi et al., 2005b). Comparison between the measured temperature profiles and CO_2 condensation temperatures reveals that temperatures below the altitude of 50 km do not fall below the condensation temperature, which confirms that the detected CO_2 ice clouds occur above 50 km.

4. Comparison with synthetic spectra from a radiative transfer model

We have performed radiative transfer calculations to reproduce the spectral shapes of the mesospheric CO_2 ice clouds measured by PFS. We used a fast and accurate radiative transfer model that includes multiple scattering effects (Ignatiev et al., 2005). CO_2 ice clouds and CO_2 gas are taken into account in the calculations, and the model atmosphere is divided into 100 layers with uniform thicknesses of 1 km. The single scattering parameters (i.e., extinction coefficient, single-scattering albedo, and scattering phase function) of the CO_2 ice clouds were calculated with the Mie theory based on the assumption of a spherical particle shape (Wiscombe, 1980). The Mie

theory calculation requires refractive indices as an input parameter. To date, two measurements of the refractive indices of CO_2 ice have been made under temperatures relatively close to those of the Martian mesosphere; one of these was the measurement of Warren (1986) taken at 65–80 K (hereafter "Warren RI"), and the other was that of Wood and Roux (1982) taken at 80 K (hereafter "Wood RI"). **Fig. 4** compares these refractive indices in the spectral range between 4.20 and 4.42 μm. Both of these indices were tested for this study. For the size distribution of CO_2 ice crystals, a lognormal distribution was adopted. The absorption coefficients of CO_2 gas were calculated based on the line-by-line method with a spectral sampling of 0.0003 cm^{-1} using the HITRAN 2012 database (Rothman et al., 2013). For the line shape function of the gas, a Voigt function was adopted (Kuntz, 1997; Ruyten, 2004). We used the solar spectrum obtained by Fiorenza and Formisano (2005). Surface albedo was assumed to be independent of wavelength and set to 0.15. Although surface albedo is variable with area, it does not impact the spectral shape at the bottom of the 4.3 μm CO_2 band because the reflection of solar radiance from the surface is completely absorbed by CO_2 gas~~es~~ in the cases selected for this study.

We assumed that the spectral feature of the mesospheric CO_2 ice clouds at the bottom of the 4.3-μm CO_2 band could be reproduced through variation of the following three parameters: optical depth τ of CO_2 clouds (reference wavelength: 1 μm), effective radius r_{eff}, and effective variance v_{eff}. The synthetic spectra were computed for combinations of the following parameters: τ = [0.01, 0.1, 0.3, 0.6, 0.9, 1.2]; r_{eff} = [0.1, 0.5, 1.0, 3.0 μm]; v_{eff} = [0.1, 0.5, 1.0]. Based on the previous observations, we have considered three scenarios with clouds distributed uniformly within three ranges of altitudes (Scholten et al., 2010): (1) 80–85 km, (2) 70–75 km, and (3) 60–65 km. Temperature and pressure profiles of the Martian atmosphere that satisfy the median conditions of the detected CO_2 clouds [Ls = 20°; latitude = 0°; longitude = 0°; local time = 16 h] were extracted from the Mars Climate Database 5.2 (Millour et al., 2015). Because the optical properties of the CO_2 ice clouds used in this study are independent of variations in temperature and pressure, we consider only the median atmospheric conditions.

Figure 5 shows typical examples of comparisons between the CO_2 cloud features measured by PFS (the same as in **Fig. 1c**) and the synthetic spectra. In this figure, the synthetic spectra calculated with clouds at altitudes of 80–85 km and effective variance of 0.1 are shown. Our modeling could not reproduce the peak of CO_2 ice with an effective radius of 0.1 μm (**Fig. 5a** and **5e**). The synthetic spectra using Warren RI with an effective radius of 0.5 μm have a peak at 4.27 μm, which is shifted toward longer wavelengths than those measured at 4.25 μm by PFS (**Fig. 5b**). The synthetic spectra using Wood RI with r_{eff} = 0.5 μm and τ = 0.3 - 0.6 are fairly similar to the measured spectra, and these values are close to the previous works by OMEGA (r_{eff} = 1-3 μm, and

$\tau < 0.5$ (Määttänen et al. 2010)) and CRISM (r_{eff} = 0.5-2 μm, and $\tau < 0.3$ (Vincendon et al. 2011)). However, the peak positions of the synthetic spectra are slightly shifted toward shorter wavelengths (4.245 μm) than that measured by PFS (4.25 μm), and the secondary peak positions of the synthetic spectra are also slightly shifted toward shorter wavelengths (4.275 μm) than that measured by PFS (4.28 μm) (**Fig. 5f**). With an effective radius larger than 1.0 μm, the synthetic spectra show significantly higher radiance in spectral ranges longer than 4.3 μm, which resulted in failure to reproduce measurements in the corresponding spectral range (**Fig. 5c**, **5d, 5g**, and **5h**). Changing the altitude of the cloud, or the effective variance of the particle size distribution, do not impact the shape of the synthetic spectra (not shown).

5. Discussion of the spectral shapes of the CO_2 ice clouds

We have compared the spectral shapes of mesospheric CO_2 ice clouds measured by PFS and synthetic spectra calculated using a radiative transfer model that assumes a spherical particle shape. As illustrated in **Fig. 5**, although the synthetic spectra with Wood RI, r_{eff} = 0.5 μm, and τ = 0.3-0.6 is fairly similar to the measured spectra, the CO_2 ice cloud features measured by PFS cannot be reproduced by the simulations. This is true for all CO_2 cloud spectra measured by PFS. **Fig. 6** shows the wavelength and intensity of the main peak of the CO_2 ice cloud features measured by PFS, as well as those of the synthetic spectra calculated with the radiative transfer model. In all cases, the main measured peaks occur between 4.24 and 4.265 μm, and none of the synthetic spectra show agreement with those peaks. Montmessin et al. (2007) also pointed out this disagreement. They used a different radiative transfer solver from ours, and calculated single scattering parameters of the CO_2 ice clouds with the Mie theory using the refractive index of Warren (1986). Their modeled peak wavelength was located at 4.28 μm, whereas the peak position observed by OMEGA was shifted by 0.02 μm toward shorter wavelengths (4.26 μm), which is consistent with our results.

In this study, two refractive indices of CO_2 ice measured at temperatures relatively close to those of the Martian mesosphere (Warren, 1986; Wood and Roux, 1982) were used for the Mie scattering calculation. However, none of the calculation results could reproduce the observed peak position, although Wood RI reproduced more similar spectra because of the double peaks (**Fig. 5f**). As shown in **Fig. 4**, the peaks of the real part of the refractive indices are located at 4.277 μm and 4.263 μm for Warren RI and Wood RI, respectively. Because the scattering coefficient at a given wavelength calculated with the Mie theory is a function of the size parameter and complex refractive index, the peak wavelength of the scattering coefficient may differ from that of the real part of index. At the 4.3-μm band, the peaks of the synthetic spectra appear at 4.27 μm with

370 Warren RI and at 4.245 μm and 4.28 μm with Wood RI (double peak) because of a combination of
371 a strong increase in absorption (i.e., the imaginary part of the index) at these spectral ranges and
372 large fluctuation of the real part when the effective radius is smaller than 0.5 μm. The
373 disagreement of the main peak wavelength between measured and synthetic spectra may arise
374 because the available CO_2 ice refractive indices are either inaccurate or inappropriate for the
375 mesospheric temperatures. In fact, the available CO_2 ice refractive indices have large uncertainties
376 in the position and width of the peak at 4.3 μm (Wood and Roux, 1982; Warren, 1986). Moreover,
377 the CO_2 condensation temperature at the altitudes of 60–100 km on Mars ranges from 95 to 120 K
378 (e.g., Listowski et al., 2014), whereas the refractive indices were measured at 65–80 K (Warren,
379 1986) and 80 K (Wood and Roux, 1982). Warren (1986) pointed out that the positions, strengths,
380 and widths of the lines in the refractive index are generally temperature dependent. Accurate
381 measurements of the refractive index with consideration for temperature dependence are needed to
382 draw a more definitive conclusion. Another possible explanation for the disagreement may be the
383 assumption in our model that the CO_2 ice crystals are spherical and composed by pure CO_2 ice.
384 While there are no ~~direct~~ observations of the cloud particles shape, the crystal shape is expected to
385 be closer to cubes or octahedrons as suggested by experiments and theoretical works (Foster et al.,
386 1998; Wood, 1999; Mangan et al., 2017), and the nucleation of CO_2 ice crystals is most probably
387 heterogeneous meaning that the crystal properties could be affected by dust grain inclusions
388 (Wood 1999; Colaprete and Toon, 2003; Määttänen et al. 2005; Listowski et al. 2014). Isenor et al.
389 (2013) demonstrated that spectral shape of the 4.3-μm band is variable depending on particle size,
390 shape, and composition (pure and mixed CO_2 aerosol particles) of the CO_2 ice ~~clouds~~ crystal using
391 the discrete dipole approximation (DDA). ~~although~~ The PFS spectra cannot be compared with
392 those of their simulation because they showed extinction spectra, which are not comparable to the
393 Nadir PFS spectra but to occultation measurements.
394 We observed a secondary peak at 4.28 μm eight times out of 111 occurrences. These occurrences
395 have no specific characteristic in observation geometry (such as phase angle, local time, latitude,
396 longitude, and season). Wood RI allows us to reproduce the double peak spectral signature (**Fig.**
397 **5f**), however, the modeled peak positions and intensities are not consistent with the observations.
398 **Fig. 7** shows relationships between secondary peak positions and radiances of the measured and
399 synthetic spectra for the eight cases. As shown in this figure, the main peak positions of the
400 synthetic spectra are slightly shifted toward shorter wavelengths (around 4.245 μm) than that
401 measured by PFS (around 4.25 μm), and the secondary peak positions of the synthetic spectra are
402 also slightly shifted toward shorter wavelengths (around 4.275 μm) than that measured by PFS
403 (around 4.28 μm). Although this discrepancy may be related to the ~~morphology~~ characteristics

(particle size, shape, and composition) of the mesospheric CO_2 ice clouds, investigating the reason for this secondary peak is beyond the scope of this paper.

The other secondary peak observed by OMEGA (Montmessin et al., 2007) in the spectral range 4.32 μm was not detected from the PFS dataset. This secondary peak is an indication of large particles (effective radius of more than 1 μm (Montmessin et al., 2007), if we assume the shape of the particle is spherical ~~(see **Fig. 5**)~~. **Fig. 6** of Määttänen et al. (2010) showed that CO_2 ice clouds with large secondary peaks (the reddish points) are spatially localized: single or a few pixels. The FOV of PFS is about 500 times larger than that of single pixel of OMEGA. Even though we could not give a general statement since **Fig. 6** of Määttänen et al. (2010) is just one example of tens of clouds that have large secondary peaks observed by OMEGA, the horizontal scale of the clouds with secondary peak at 4.32-34 μm may be too small to be detected by PFS.

6. Conclusion

In this study, we have identified 111 occurrences of mesospheric CO_2 ice clouds at the bottom of the 4.3-μm CO_2 band from PFS measurements over the period from MY 27 to MY 32. Detections of CO_2 ice clouds were compared with those observed by OMEGA (Määttänen et al., 2010; Vincendon et al., 2011) and all cases of simultaneous observations (51 cases) were also confirmed by OMEGA data. The spatial distribution of the mesospheric CO_2 ice clouds shows that they occur within the longitudinal range of −100.6°E to +23.2°E (109 cases) and around +161°E (2 cases) over the equatorial latitudes (15.6°S–21.5°N). The seasonal distribution indicates that they occurred within the seasonal range of Ls = 8.9° to 134.6°, concentrated between Ls = 10° and 30° (87 cases). The season and locations in which mesospheric CO_2 ice clouds were detected are consistent with previous spectroscopic observations (Määttänen et al., 2010; Vincendon et al., 2011). Moreover, mesospheric CO_2 ice clouds were found preferentially in the spectra taken in the late afternoon (15–16 h) in MY 29 even though this cannot be generalized because of the observational biases. ~~The global dust storm occurred at the northern fall in MY 28 could not be ruled out as a possible explanation for this. Our calculation shows that small dust particles (of the order of a few nm) can remain suspended in the mesosphere for a relatively long time and act as condensation nuclei of the CO_2 ice clouds.~~

The high spectral resolution of PFS enables us to resolve the spectral shape of CO_2 ice clouds for the first time. In all cases, the CO_2 ice scattering peak is located at 4.25 μm (between 4.240 and 4.265 μm), which is consistent with observation by OMEGA (Monemessin et al., 2007). Moreover, a small secondary peak is found around 4.28 μm (eight occurrences), which was not resolved by OMEGA. The other secondary peak observed by OMEGA (Montmessin et al., 2007)

in the spectral range 4.32–4.34 μm ~~cannot be~~ was not detected by PFS. We have compared the spectral shapes of mesospheric CO_2 ice clouds measured by PFS and synthetic spectra calculated using a radiative transfer model that assumes a spherical particle shape. Two refractive indices of CO_2 ice measured at temperatures relatively close to those for the Martian mesosphere (Warren, 1986; Wood and Roux, 1982) were used for the Mie scattering calculation. The synthetic spectra with Wood RI, r_{eff} = 0.5 μm and τ = 0.3-0.6 is more similar to the measured spectra and only Wood RI allows to reproduce a double peak structure like the one detected in a few spectra. However, none of the calculated synthetic spectra show agreement with the measured shape of the spectra and positions of the peaks. This disagreement may be because (1) the available CO_2 ice refractive indices are either inaccurate or inappropriate for the mesospheric temperatures, or (2) because of the assumption in our model that the CO_2 ice crystals are spherical and composed by pure CO_2 ice. The discrete dipole approximation (DDA), which is widely used for non-spherical particles modeling in astronomy and planetary science and was used in the simulation demonstrated by Isenor et al. (2013), ~~is able~~ would allow us to model IR spectra of non-spherical crystals to be compared with the PFS spectra. Detailed comparison between the measured PFS spectra and those modeled by the DDA ~~(including the reason for the secondary peak)~~ ~~will~~ can provide new insight on the ~~morphology~~ microphysical characteristics of these mesospheric CO_2 ice clouds.

Acknowledgements

This work has been supported by the European Union Seventh Framework Programme (FP7/2007-2013) under grant agreement n° 607177, FNRS “CRAMIC” project under grant agreement n° T.0171.16, a Grant-in-Aid for Scientific Research (22340142, 24403007, 15H05209, 16K05566) from the Japanese Society for the Promotion of Science (JSPS), and the Tohoku University Global COE program "Global Education and Research Center for Earth and Planetary Dynamics". Mars Express (MEx) has been operated by the ESA, and we are grateful to the MEx-SGS team for their support. The Mars Climate Database 5.2 is provided by F. Forget and E. Millour. The MEx/OMEGA data set was obtained from the Planetary Data System (PDS).

Reference

~~Berger, U., Hartogh, P., Meister C.-V., Villanueva, G., 2003. Hydrodynamic Model of the Martian Atmosphere between Near-Surface Layers and an Altitude of about 130 km, Astronomische Nachrichten, Supplementary Issue 2, Vol. 324, Short Contributions of the Annual Scientific Meeting of the Astronomische Gesellschaft in Berlin, September 23-28, 2002, p.57~~

Bibring, J-P., Soufflot, A., Berthé, M., Langevin, Y., Gondet, B., Drossart, P., Bouyé, M., Combes, M., Puget, P., Semery, A., Bellucci, G., Formisano, V., Moroz, V., Kottsov, V., the OMEGA Co-I team. 2004. OMEGA: Observatoire pour la Mine´ralogie, l'Eau, les Glaces et l'Activite´, in Mars Express: The Scientific Payload, Eur. Space Agency Spec. Publ., ESA-SP 1240, 37–50.

Clancy, R.T., Sandor, B.J., 1998. CO_2 ice clouds in the upper atmosphere of Mars. Geophys. Res. Lett. 25 (4), 489–492.

Colaprete, A., and Toon O.B., 2003. Carbon dioxide clouds in an early dense Martian atmosphere. Journal of Geophysical Research (Planets), Volume 108, Issue E4, pp. 6-1

Foster, J.L., Chang, A.T.C., Hall, D.K., Wergin, W.P., Erbe, E.F., Barton, J., 1998. Carbon dioxide crystals: An examination of their size, shape, and scattering properties at 37 GHz and comparisons with water ice (snow) measurements. Journal of Geophysical Research, Volume 103, Issue E11, p. 25839-25850

Formisano, V., Angrilli, F., Arnold, G., Atreya, S., Bianchini, G., Biondi, D., Blanco, A., Blecka, M.I., Coradini, A., Colangeli, L., Ekonomov, A., Esposito, F., Fonti, S., Giuranna, M., Grassi, D., Gnedykh, V., Grigoriev, A., Hansen, G., Hirsh, H., Khatuntsev, I., Kiselev, A., Ignatiev, N., Jurewicz, A., Lellouch, E., Lopez Moreno, J., Marten, A., Mattana, A., Maturilli, A., Mencarelli, E., Michalska, M., Moroz, V., Moshkin, B., Nespoli, F., Nikolsky, Y., Orfei, R., Orleanski, P., Orofino, V., Palomba, E., Patsaev, D., Piccioni, G., Rataj, M., Rodrigo, R., Rodriguez, J., Rossi, M., Saggin, B., Titov, D., Zasova, L., 2005. The Planetary Fourier Spectrometer (PFS) onboard the European Mars Express mission. Planet. Space Sci. 53 (10), 963–974.

Formisano, V., Maturilli, A., Giuranna, M., D'Aversa, E., Lopez-Valverde, M.A., 2006. Observations of non-LTE emission at 4-5 microns with the planetary Fourier spectrometer aboard the Mars Express mission, Icarus, 182, 51–67.

Fiorenza, C., Formisano, V., 2005. A solar spectrum for PFS data analysis. Planet. Space Sci. 53, 1009–1016.

Giuranna, M., Formisano, V., Biondi, D., Ekonomov, A., Fonti, S., Grassi, D., Hirsch, H., Khatuntsev, I., Ignatiev, N., Michalska, M., Mattana, A., Maturilli, A., Mencarelli, E., Nespoli, F., Orfei, R., Orleanski, P., Piccioni, G., Rataj, M., Saggin, B., Zasova, L., 2005a. Calibration of the Planetary Fourier Spectrometer long wavelength channel. Planet. Space Sci. 53 (10), 993–1007.

Giuranna, M., Formisano, V., Biondi, D., Ekonomov, A., Fonti, S., Grassi, D., Hirsch, H., Khatuntsev, I., Ignatiev, N., Michalska, M., Mattana, A., Maturilli, A., Moshkin, B.E., Mencarelli, E., Nespoli, F., Orfei, R., Orleanski, P., Piccioni, G., Rataj, M., Saggin, B., Zasova,

L., 2005b. Calibration of the Planetary Fourier Spectrometer short wavelength channel. Planet. Space Sci. 53 (10), 975–991.

González-Galindo, F., Määttänen, A., Forget, F., Spiga, A., 2011. The martian mesosphere as revealed by CO_2 cloud observations and general circulation modeling. Icarus 216, 10–22.

Grassi, D., Fiorenza, C., Zasova, L.V., Ignatiev, N.I., Maturilli, A., Formisano, V., Giuranna, M., 2005. The martian atmosphere above great volcanoes: early planetary fourier spectrometer observations, Planet. Space Sci., 53, 1017-1034.

Grassi, D., Ignatiev, N.I., Zasova, L.V., Maturilli, A., Formisano, V., Bianchini, G.A., Giuranna, M., 2005b. Methods for the analysis of data from the Planetary Fourier Spectrometer on the Mars Express mission. Planet. Space Sci., 53, 1053-1064.

~~Guzewich, S.D., Talaat, E.R., Toigo, A.D., Waugh, D.W., McConnochie, T.H., 2013. High-altitude dust layers on Mars: Observations with the Thermal Emission Spectrometer, Journal of Geophysical Research: Planets, vol. 118, 1177-1194.~~

Herr, K. C., and Pimentel, G. C., 1970. Evidence for solid carbon dioxide in the upper atmosphere of Mars, Science, 167, 47–49,

Ignatiev, N.I., Grassi, D., Zasova, L.V., 2005. Planetary Fourier spectrometer data analysis: fast radiative transfer models. Planet. Space Sci. 53, 1035–1042.

Isenor, M, Escribano, R., Preston, T.C., Signorell, R., 2013. Predicting the infrared band profiles for CO_2 cloud particles on Mars. Icarus, 223, 591–601.

Kahre M.A., Hollingsworth, J.L., Haberle, R.M., Murphy, J.R., 2008. Investigations of the variability of dust particle sizes in the martian atmosphere using the NASA Ames General Circulation Model, Icarus, 195, 576-597

Kuntz, M., 1997. A new implementation of the Humlicek algorithmfor the calculation of the Voigt profile function. J. Quant. Spectrosc. Radiat. Transfer 57 (6), 819–824.

Lellouch, E., Encrenaz T., de Graauw T., Erard S., Morris P., Crovisier J., Feuchtgruber H., Girard T., Burgdorf M., 2000. The 2.4– 45 mm spectrum of Mars observed with the infrared space observatory, Planet. Space Sci., 48, 1393–1405.

Lewis S.R. and Steele, L.J., 2014. High-Altitude Dust in the Martian Atmosphere, Mars Modeling and Observations Workshop, London, 2014

Listowski, C., Määttänen, A., Montmessin, F., Spiga, A., Lefevre, F., 2014. Modeling the microphysics of CO_2 ice clouds within wave-induced cold pockets in the Martian mesosphere, Icarus, 237, 239–261.

Määttänen, A., Vehkamäki, H., Lauri, A., Merikallio, S., Kauhanen, J., Savijärvi, H., Kulmala, M., 2005. Nucleation studies in the Martian atmosphere. Journal of Geophysical Research, Volume

110, Issue E2, CiteID E02002.

Määttänen, A., Montmessin, F., Gondet, B., Scholten, F., Hoffmann, H., González- Galindo, F., Spiga, A., Forget, F., Hauber, E., Neukum, G., Bibring, J.-P., Bertaux, J.-L., 2010. Mapping the mesospheric CO_2 clouds on Mars: MEx/OMEGA and MEx/HRSC observations and challenges for atmospheric models. Icarus 209, 452–469.

Mangan, T.P., Salzmann, C.G., Plane, J.M.C., Murray, B.J., 2017. CO2 ice structure and density under Martian atmospheric conditions. Icarus, Volume 294, p. 201-208.

Millour, E. et al., 2015. The Mars Climate Database (MCD version 5.2). European Planetary Science Congress 2015, id.EPSC2015-438.

Montmessin, F., Bertaux, J.-L., Quémerais, E., Korablev, O., Rannou, P., Forget, F., Perrier, S., Fussen, D., Lebonnois, S., Rébérac, A., Dimarellis, E., 2006. Subvisible CO_2 ice clouds detected in the mesosphere of Mars. Icarus 183, 403–410.

Montmessin, F., Gondet, B., Bibring, J.-P., Langevin, Y., Drossart, P., Forget, F., 2007. Hyperspectral imaging of convective CO_2 ice clouds in the equatorial mesosphere of Mars. J. Geophys. Res. 112 (E11S90), 1–14.

~~Murphy J.R., Toon, O.B., Haberle, R.M., Pollack, J.B., 1990. Numerical Simulations of the Decay of Martian Global Dust Storms. Journal of Geophysical Research, vol. 95, NO. B9, 14629-14648.~~

~~Murphy J.R., Haberle, R.M., Toon O.B., Pollack, J.B., 1993. Martian Global Dust Storms: Zonally Symmetric Numerical Simulations Including Size-Dependent Particle Transport. Journal of Geophysical Research, vol. 98, NO. E2, 3197-3220.~~

Rothman, L.S., Gordon, I.E., Babikov, Y., Barbe, A., Chris Benner, D., Bernath, P.F., Birk, Bizzocchi, L., Boudon, V., Brown, L.R, Campargue, A., Chance, K., Cohen, E.A., Coudert, L.H., Devi, V.M., Drouin, B.J., Fayt, A., Flaud, J.-M., Gamache, R.R., Harrison, J.J., Hartmann, J.-M., Hill, C., Hodges, J.T., Jacquemart, D., Jolly, A., Lamouroux, J., Le Roy, R.J., Li, G., Long, D.A., Lyulin, O.M., Mackie, C.J., Massie, S.T., Mikhailenko, S., 2013. The HITRAN2012 molecular spectroscopic database. J. Quant. Spectrosc. Radiat. Transfer 130, 4-50.

Ruyten, W., 2004. Comment on ‘‘A new implementation of the Humlicek algorithm for the calculation of the Voigt profile function’’ by M. Kuntz [JQSRT 57(6) (1997) 819–824]. J. Quant. Spectrosc. Radiat. Transfer 86, 231–233.

Schofield, J.T. et al., 1997. The Mars pathfinder atmospheric structure investigation/ meteorology (ASI/MET) experiment. Science 278, 1752–1757.

Scholten, F., Hoffmann, H., Määttänen, A., Montmessin, F., Gondet, B., Hauber, E., 2010.

Concatenation of HRSC colour and OMEGA data for the determination and 3d-parameterization of high-altitude CO_2 clouds in the martian atmosphere. Planet. Space Sci. 58, 1207–1214.

Spiga, A., González-Galindo, F., López-Valverde, M.-Á., Forget, F., 2012. Gravity waves, cold pockets and CO_2 clouds in the martian mesosphere. Geophys. Res. Lett. 39 (L02201), 1–5.

Smith, M. D., 2009. THEMIS observations of Mars aerosol optical depth from 2002 – 2008, Icarus, 202, 444 – 452.

Vincendon, M., Pilorget, C., Gondet, B., Murchie, S., Bibring, J.-P., 2011. New near-ir observations of mesospheric CO_2 and H_2O clouds on Mars. J. Geophys. Res. 116 (E00J02), 1–30.

Warren, S.G., 1984. Optical constants of ice from the ultraviolet to the microwave. Appl. Opt. 23, 1206–1225.

Wiscombe, W.J., 1980. Improved Mie scattering algorithms. Applied Optics, 19, 9, 1505–1509.

Wolkenberg, P., Giuranna, M., Grassi, D., Aronica, A., Aoki, S., Scaccabarozzi, D., Saggin, B., 2017. Characterization of dust activity on Mars from MY 27 to MY 32 by PFS-MEX observations. Icarus, submitted (under revision).

Wood, B.E., Roux, J.A., 1982. Infrared Optical Properties of Thin H_2O, NH_3, and CO_2 Cryofilms. J. Opt. Soc. Am. 72,720.

Wood, S.E., 1999. Nucleation and growth of carbon dioxide ice crystals in the Martian atmosphere. Thesis (PhD). UNIVERSITY OF CALIFORNIA, LOS ANGELES, Source DAI-B 60/04, p. 1653, Oct 1999, 192 pages.

Figures and Table

Figure 1: Examples of PFS spectra in the wavelength range between 4.0 μm and 4.5 μm (black curves). The light green and blue curves represent the estimated background radiance and the best-fit quadratic function in the spectral range 4.22–4.35 μm, respectively. The red curves show the smoothed PFS spectra. (a) An example of a PFS spectrum without mesospheric CO_2 ice cloud features (d_1 = 0.029, d_2 = 0.097, orbit #886, latitude = 44.57°N, longitude = 19.44°E, and *Ls* = 93.33°). (b) An example of PFS spectra with mesospheric CO_2 ice cloud features identified by the algorithm (d_1 = 0.108, d_2 = 3.522, orbit # 5267, latitude = 2.88°S, longitude = +17.27°E, and Ls = 28.69°). (c) An example of PFS spectra with mesospheric CO_2 ice cloud features with a secondary peak is found at 4.28 μm (d_1 =0.129, d_2 = 4.007, orbit #5267, latitude = 2.35°S, longitude = +17.27°E, and Ls = 28.69°). (d) An example of a "noisy" PFS spectrum without mesospheric CO_2 ice cloud features (d_1 = 0.070, d_2 = 0.491, orbit #4537, latitude = 8.02°S, longitude = −23.83°E,

608 and Ls = 277.92°). A relatively high noise level provides a large d_1 value, although a distinct
609 scattering peak is not visible. (e) An example of a PFS spectrum with mesospheric CO_2 ice cloud
610 features not detected by algorithm but only by eye (d_1 = 0.054, d_2 = 0.503, orbit #5195, latitude =
611 7.01°N, longitude = +22.52°E, and Ls = 19.13°). A possible CO_2 ice cloud feature is visible around
612 4.25 μm.
613
614 Figure 2: (Top) Spatial distribution of the mesospheric CO_2 ice clouds observed by MEx/PFS. The
615 colors relate to the solar longitude. (Bottom) Seasonal distributions of mesospheric CO_2 ice clouds.
616
617 Figure 3: (a) Local time of the PFS spectra used in this study as a function of Ls (x-axis) and
618 latitude (y-axis) in the different MYs (MY27-32). Only daytime observations (between 6 and 18)
619 taken at low-middle latitudes (70°S-70°N) are shown here. (b) Number of mesospheric CO_2 ice
620 clouds detected by PFS at 1-h intervals between 8 and 18 h. (c) Detection probability of
621 mesospheric CO_2 ice clouds at 1-h intervals between 8 and 18 h. In panel c, only detections within
622 the latitudes of 20°S–20°N, longitudes of −110°E to +30°E, and season of Ls = 10–30° were used
623 for these statistics to exclude observational biases. Differences in color represent the observational
624 MY.
625
626 Figure 4: Refractive indices of CO_2 ice used for the Mie scattering calculation performed in this
627 study. The red and blue curves represent the indices by Warren (1986) and by Wood and Roux
628 (1982), respectively. The solid curves indicate the real parts of the indices, and the dashed curves
629 represent the imaginary parts.
630
631 Figure 5: Examples of the comparison between measured mesospheric CO_2 ice cloud spectral
632 features and synthetic spectra calculated using the CO_2 ice refractive indices of Warren (1986)
633 (Figs. a–d) and Wood and Roux (1982) (Figs. e–f). The black curves show a typical example of a
634 CO_2 ice cloud spectrum observed by PFS with a spectrum showing a clear secondary peak at 4.28
635 μm (same as that shown in Fig. 1c). The synthetic spectra were calculated with various effective
636 radii: r_{eff} = [0.1, 0.5, 1.0, 3.0 μm]. The effective radius v_{eff} of the size distribution is assumed to be
637 0.1. The purple, blue, light blue, green, orange, and red curves represent the synthetic spectra with
638 optical depths of τ = [0.01, 0.1, 0.3, 0.6, 0.9, 1.2], respectively. Cloud altitudes were assumed to be
639 distributed uniformly within the altitudes of 80–85 km.
640
641 Figure 6: Relationships between main peak positions and radiance of the measured (red) and

642 synthetic spectra (other colors) calculated with (a) the refractive index of Warren (1986), and (b)
643 that of Wood and Roux (1982). The black and blue diamonds, triangles, and squares represent the
644 values of the synthetic spectra with the optical depths of τ = [0.3, 0.6, 0.9] and the effective
645 variance V_{eff} = 0.1 and the effective radius R_{eff} = 0.5 μm (black) and 1.0 μm (blue), respectively.
646
647 Figure 7: Relationships between secondary peak positions and radiances of the measured (circles)
648 and synthetic (other symbols) spectra for the eight cases (in different colors). The synthetic spectra
649 shown here are those calculated with the refractive index of Wood and Roux (1982), R_{eff} = 0.5 μm
650 and V_{eff} = 0.1. The diamonds, triangles, and squares represent the values of the synthetic spectra
651 with optical depths of τ = [0.3, 0.6, 0.9], respectively. Note that the black and red open symbols
652 (synthetic spectra) sit on the top of each other because solar zenith angles during the observations
653 are similar.
654
655 ~~Figure 8: Difference between radiance at 4.26 μm and 4.32 μm in the OMEGA spectra acquired~~
656 ~~within the PFS FOV during the simultaneous detection of the CO_2 ice clouds by PFS and~~
657 ~~OMEGA. X-axis shows the difference and Y-axis is the number of OMEGA spectra.~~

658 Table 1. List of the mesospheric CO_2 ice clouds detected by PFS during the period from MY 27 to
659 MY 32. The cross symbols in the eighth column indicate that the detections are also confirmed by
660 OMEGA (i.e., reported by Määttänen et al. (2010) and Vincendon et al. (2011)), the minus
661 symbols signify that OMEGA was not operating, and question marks indicate that analysis with
662 the OMEGA data has not yet been reported. The cross symbols in the last column indicate spectra
663 with a secondary peak at 4.28 μm.
664

MEx Orbit#	Obs. #	Latitude (°N)	Longitude (°E)	Local Time	Martian Year	Ls (°)	OMEGA Detection	4.28 μm Peak
1205	184	0.22	-7.95	13.5	27	134.59	+	+
2890	312	21.48	22.3	17.87	28	37.91	-	
5120	135	-1.73	-34.56	16.66	29	8.9	+	
5135	134	2.16	-95.06	16.52	29	10.97	-	
5167	139	5.62	-56.64	16.2	29	15.34	-	
5170	150	-0.23	3.65	16.22	29	15.75	+	
5170	153	-1.91	3.64	16.23	29	15.75	+	
5177	160	-4.72	23.22	16.17	29	16.7	+	
5189	128	-4.79	-97.61	16.04	29	18.32	-	
5189	129	-5.35	-97.62	16.04	29	18.32	-	
5189	130	-5.91	-97.62	16.04	29	18.32	-	
5195	115	1.84	22.5	15.97	29	19.13	-	
5195	116	1.26	22.5	15.97	29	19.13	-	
5195	117	0.68	22.49	15.98	29	19.13	-	
5195	118	0.17	22.49	15.98	29	19.13	-	
5195	119	-0.4	22.49	15.98	29	19.13	-	
5195	120	-0.98	22.48	15.98	29	19.13	-	
5195	121	-1.55	22.48	15.99	29	19.13	-	
5195	123	-2.69	22.48	15.99	29	19.13	-	
5195	124	-3.2	22.47	15.99	29	19.13	-	
5195	133	-8.2	22.45	16.01	29	19.13	-	
5196	21	-2.7	-78.14	15.94	29	19.26	-	
5196	22	-3.2	-78.15	15.94	29	19.26	-	+
5196	23	-3.77	-78.15	15.95	29	19.26	-	

5206	105	8.5	1.63	15.82	29	20.6	+	+
5206	106	7.92	1.63	15.82	29	20.6	+	
5207	107	7.6	-98.34	15.82	29	20.74	-	
5207	108	7.02	-98.34	15.82	29	20.74	-	
5208	133	-6.88	161.45	15.86	29	20.87	-	
5208	143	-12.26	161.41	15.89	29	20.87	-	
5213	124	2.17	21.14	15.77	29	21.54	-	
5213	125	1.60	21.14	15.78	29	21.54	-	
5213	148	-11.01	21.05	15.83	29	21.54	-	
5214	134	-2.74	-78.78	15.8	29	21.68	-	
5224	126	3.05	0.76	15.69	29	23.01	+	+
5225	134	-0.87	-99.45	15.68	29	23.14	+	
5225	162	-15.59	-99.57	15.74	29	23.14	+	
5231	2	-1.35	19.79	15.6	29	23.94	+	
5231	4	-2.45	19.78	15.61	29	23.94	+	
5231	6	-3.54	19.77	15.61	29	23.94	+	
5231	7	-4.08	19.77	15.61	29	23.94	+	
5231	8	-4.62	19.76	15.61	29	23.94	+	
5231	10	-5.70	19.75	15.62	29	23.94	+	
5231	12	-6.72	19.74	15.62	29	23.94	+	
5231	13	-7.25	19.74	15.63	29	23.94	+	
5231	19	-10.41	19.71	15.64	29	23.94	+	
5232	145	-5.76	-80.04	15.63	29	24.07	+	
5243	152	-6.99	-100.62	15.54	29	25.53	-	
5243	153	-7.52	-100.62	15.54	29	25.53	-	
5243	155	-8.56	-100.63	15.55	29	25.53	-	
5249	124	9.86	18.63	15.38	29	26.32	-	
5249	142	-0.07	18.58	15.42	29	26.32	-	
5250	143	-0.57	-81.18	15.44	29	26.45	-	
5250	145	-1.65	-81.19	15.44	29	26.45	-	
5250	157	-7.87	-81.25	15.47	29	26.45	-	
5257	137	3.73	-61.56	15.36	29	27.38	+	
5257	138	3.18	-61.56	15.36	29	27.38	+	

5257	140	2.08	-61.57	15.36	29	27.38	+	
5257	142	0.99	-61.58	15.37	29	27.38	+	
5257	143	0.5	-61.58	15.37	29	27.38	+	
5257	144	-0.04	-61.59	15.37	29	27.38	+	
5257	145	-0.58	-61.59	15.37	29	27.38	+	
5257	146	-1.12	-61.6	15.37	29	27.38	+	
5257	148	-2.19	-61.61	15.38	29	27.38	+	
5257	150	-3.19	-61.62	15.38	29	27.38	+	
5267	136	5.63	17.34	15.22	29	28.69	+	
5267	138	4.59	17.34	15.23	29	28.69	+	
5267	139	4.04	17.33	15.23	29	28.69	+	+
5267	140	3.49	17.33	15.23	29	28.69	+	
5267	141	2.95	17.32	15.23	29	28.69	+	
5267	142	2.4	17.32	15.24	29	28.69	+	
5267	145	0.78	17.31	15.24	29	28.69	+	
5267	148	-0.76	17.29	15.25	29	28.69	+	+
5267	149	-1.3	17.29	15.25	29	28.69	+	
5267	150	-1.83	17.28	15.25	29	28.69	+	
5267	151	-2.35	17.27	15.25	29	28.69	+	+
5267	152	-2.88	17.27	15.26	29	28.69	+	
5267	153	-3.4	17.26	15.26	29	28.69	+	
5267	154	-3.92	17.26	15.26	29	28.69	+	
5267	155	-4.44	17.25	15.26	29	28.69	+	
7529	158	8.92	-5.31	13.4	30	10	-	
7529	162	7.18	-5.36	13.41	30	10	-	
7529	179	0.25	-5.59	13.44	30	10	-	
7529	180	-0.12	-5.6	13.44	30	10	-	
7529	182	-0.9	-5.63	13.44	30	10	-	
7561	138	0.18	7.96	13.22	30	14.42	-	
7561	140	-0.79	7.96	13.22	30	14.42	-	
7561	142	-1.75	7.96	13.23	30	14.42	-	
7643	198	-4.27	18.07	12.52	30	25.51	-	
7668	33	-8.68	14.66	12.19	30	28.83	-	

7960	244	8.42	-10.36	9.07	30	66.31	-	
7960	245	8.12	-10.38	9.07	30	66.31	-	
7960	246	7.85	-10.4	9.07	30	66.31	-	
7960	247	7.55	-10.43	9.07	30	66.31	-	
7960	248	7.26	-10.46	9.07	30	66.31	-	
7960	249	6.96	-10.48	9.07	30	66.31	-	
7960	250	6.69	-10.51	9.08	30	66.31	-	
8020	152	8.50	-29.54	8.26	30	73.95	+	
8020	154	7.98	-29.60	8.26	30	73.95	+	
8020	155	7.74	-29.63	8.26	30	73.95	+	
8020	162	5.93	-29.83	8.27	30	73.95	+	
8020	163	5.66	-29.86	8.27	30	73.95	+	
8020	164	5.39	-29.89	8.27	30	73.95	+	
10690	100	-7.08	-26.83	14.2	31	114.51	?	
10690	102	-6.19	-26.86	14.2	31	114.51	?	
13050	127	-2.47	-17.23	11.2	32	114.62	-	
13050	128	-2.14	-17.25	11.2	32	114.62	-	
13050	129	-1.87	-17.27	11.2	32	114.62	-	
13050	130	-1.54	-17.3	11.2	32	114.62	-	+
13050	131	-1.24	-17.32	11.21	32	114.62	-	
13050	132	-0.94	-17.34	11.21	32	114.62	-	

Appendix A. Possible detections of mesospheric CO_2 ice clouds

We have identified 111 occurrences of mesospheric CO_2 ice clouds at the bottom of the 4.3-μm CO_2 band from the PFS dataset using the algorithm described in Section 2.2. However, this algorithm is conservative, and will certainly exclude possible CO_2 cloud detections with weaker signals. Therefore, we have visually inspected the entire PFS dataset to search for other possible CO_2 ice cloud occurrences. As a result, we have identified an additional 175 occurrences that have very similar features to the algorithm detections but were excluded because their signals are weaker and difficult to differentiate from instrumental noise. These visual detections were compared with detections in OMEGA measurements during MY 27–30 (Tables 3 and 4 in Määttänen et al., 2010; Table 3 in Vincendon et al., 2011). There were 167 detections in MY 27–30, and OMEGA performed observations during 73 of these 167 occurrences. We find that OMEGA identified mesospheric CO_2 ice cloud features during all 73 of these occurrences. The list

678 of visual CO_2 ice cloud detections is provided in **Table A1**.

679 **Figure A1** shows the spatial and seasonal distributions of mesospheric CO_2 ice clouds. The
680 visual and algorithm detections are shown together. The distributions are very similar to those of
681 the algorithm detections alone. The spatial distribution shows that the CO_2 ice clouds were
682 detected within the longitudinal range of −100.6°E to +25.2°E (282 cases) and around +161°E
683 (four cases) over the equatorial latitudes ranging from 21.4°S to 21.5°N. The seasonal distribution
684 shows that they occurred in the seasonal range between Ls = 3.5° and 134.6°, with most
685 concentrated between Ls = 10° and 30° (237 cases). The distribution of these additional detections
686 is in good agreement with that revealed by the previous and current analyses.
687
688 Figure A1: (Top) Spatial and (bottom) seasonal distributions of mesospheric CO_2 ice clouds
689 observed by MExX/PFS. Differences in color in the top map represent the measured solar
690 longitude, and the circle and cross symbols show algorithm and visual detections, respectively.
691
692
693
694
695

Table A1: List of mesospheric CO_2 ice clouds detected visually. The cross symbols in the 8th column mean that the detections are also confirmed by OMEGA (i.e., reported in Määttänen et al. (2010) and Vincendon et al. (2011)), the minus symbols represent that OMEGA was not operating, and question marks mean that analysis with the OMEGA data are not yet reported. The cross symbols in the last column indicate spectra with a secondary peak at 4.28 μm.

MEx Orbit#	Obs. #	Latitude (°N)	Longitude (°E)	Local Time	Martian Year	Ls (°)	OMEGA Detection	4.28 μm Peak
934	292	-6.68	-18.53	16.37	27	99.32	+	
945	284	0.26	-19.5	16.21	27	100.69	+	
1205	154	16.56	-7.9	13.43	27	134.59	+	+
1205	155	15.98	-7.9	13.44	27	134.59	+	
1205	156	15.4	-7.89	13.44	27	134.59	+	
1205	160	13.16	-7.89	13.45	27	134.59	+	
1205	163	11.51	-7.89	13.45	27	134.59	+	
1205	185	-0.25	-7.95	13.5	27	134.59	+	
5081	123	-0.73	-92.24	17.07	29	3.45	-	
5081	130	-4.81	-92.26	17.09	29	3.45	-	
5117	132	-0.35	-94.1	16.71	29	8.48	-	
5117	136	-2.71	-94.11	16.71	29	8.48	-	
5123	124	4.15	25.21	16.6	29	9.31	+	
5134	125	6.94	4.71	16.49	29	10.83	-	
5134	127	5.76	4.71	16.49	29	10.83	-	+
5134	128	5.24	4.71	16.5	29	10.83	-	+
5134	136	0.52	4.69	16.51	29	10.83	-	
5135	135	1.57	-95.06	16.52	29	10.97	-	
5135	137	0.39	-95.07	16.53	29	10.97	-	
5135	138	-0.2	-95.07	16.53	29	10.97	-	
5135	139	-0.78	-95.07	16.53	29	10.97	-	
5135	142	-2.55	-95.08	16.54	29	10.97	-	
5135	149	-6.57	-95.1	16.55	29	10.97	-	
5135	150	-7.15	-95.1	16.56	29	10.97	-	

5141	136	1.98	25.11	16.49	29	11.79	+	
5141	137	1.39	25.11	16.49	29	11.79	+	
5141	138	0.8	25.11	16.5	29	11.79	+	
5141	139	0.21	25.1	16.5	29	11.79	+	
5141	140	-0.38	25.1	16.5	29	11.79	+	
5141	144	-2.65	25.09	16.51	29	11.79	+	
5141	145	-3.24	25.09	16.51	29	11.79	+	
5153	138	3.48	-96.01	16.34	29	13.44	-	
5153	139	2.89	-96.01	16.34	29	13.44	-	
5153	146	-1.15	-96.03	16.36	29	13.44	-	+
5153	147	-1.73	-96.04	16.36	29	13.44	-	
5159	151	-2.56	24.16	16.34	29	14.26	-	
5167	140	5.04	-56.65	16.2	29	15.34	-	
5167	141	4.45	-56.65	16.2	29	15.34	-	
5167	142	3.93	-56.65	16.21	29	15.34	-	
5167	143	3.34	-56.65	16.21	29	15.34	-	
5167	153	-2.41	-56.68	16.23	29	15.34	-	+
5167	162	-7.5	-56.71	16.25	29	15.35	-	
5170	142	4.37	3.67	16.21	29	15.75	+	
5170	149	0.35	3.65	16.22	29	15.75	+	
5170	151	-0.75	3.65	16.23	29	15.75	+	
5170	152	-1.33	3.64	16.23	29	15.75	+	
5170	154	-2.48	3.64	16.23	29	15.75	+	
5170	155	-3.06	3.64	16.24	29	15.75	+	
5170	162	-6.99	3.62	16.25	29	15.75	+	
5170	163	-7.56	3.61	16.25	29	15.75	+	
5170	171	-11.97	3.6	16.27	29	15.75	+	
5177	158	-3.64	23.22	16.17	29	16.7	+	
5177	161	-5.29	23.21	16.17	29	16.7	+	
5177	162	-5.85	23.21	16.17	29	16.7	+	
5177	163	-6.42	23.21	16.18	29	16.7	+	
5177	164	-6.98	23.21	16.18	29	16.7	+	
5177	165	-7.55	23.2	16.18	29	16.7	+	

5177	170	-10.27	23.19	16.19	29	16.7	+	
5177	171	-10.83	23.19	16.19	29	16.7	+	
5177	172	-11.38	23.19	16.2	29	16.7	+	
5188	106	7.83	2.00	15.97	29	18.19	-	
5188	111	4.97	1.99	15.98	29	18.19	-	
5188	117	1.55	1.97	15.99	29	18.19	-	
5188	118	0.97	1.97	15.99	29	18.19	-	
5189	122	-1.43	-97.59	16.03	29	18.32	-	+
5189	123	-2.01	-97.6	16.03	29	18.32	-	
5189	131	-6.48	-97.62	16.04	29	18.32	-	
5189	134	-8.09	-97.63	16.05	29	18.32	-	
5189	136	-9.2	-97.64	16.06	29	18.32	-	
5189	137	-9.75	-97.64	16.06	29	18.32	-	
5195	106	7.01	22.52	15.95	29	19.13	-	
5195	107	6.43	22.52	15.95	29	19.13	-	
5195	108	5.84	22.52	15.96	29	19.13	-	
5195	110	4.68	22.51	15.96	29	19.13	-	
5195	111	4.16	22.51	15.96	29	19.13	-	
5195	113	3.00	22.5	15.97	29	19.13	-	
5195	114	2.42	22.5	15.97	29	19.13	-	
5195	122	-2.12	22.48	15.99	29	19.13	-	
5195	125	-3.77	22.47	15.99	29	19.13	-	
5195	126	-4.33	22.47	16	29	19.13	-	
5195	127	-4.9	22.47	16	29	19.13	-	
5195	128	-5.46	22.46	16	29	19.13	-	
5195	129	-6.02	22.46	16	29	19.13	--	
5195	130	-6.52	22.46	16	29	19.13	-	
5195	132	-7.64	22.45	16.01	29	19.13	-	
5195	135	-9.31	22.44	16.02	29	19.13	-	
5196	27	-6.03	-78.17	15.96	29	19.26	-	
5196	29	-7.15	-78.17	15.96	29	19.26	-	
5196	30	-7.65	-78.18	15.96	29	19.26	-	
5203	122	-3.31	-57.79	15.92	29	20.2	+	

5203	126	-5.57	-57.8	15.93	29	20.2	+	
5206	112	4.5	1.61	15.83	29	20.6	+	
5207	102	10.45	-98.33	15.81	29	20.74	-	
5207	110	5.86	-98.35	15.83	29	20.74	-	
5207	111	5.28	-98.35	15.83	29	20.74	-	
5207	129	-4.81	-98.41	15.87	29	20.74	-	
5207	133	-7.01	-98.43	15.88	29	20.74	-	+
5208	139	-10.13	161.43	15.88	29	20.87	-	
5208	142	-11.73	161.42	15.88	29	20.87	-	
5213	122	3.25	21.15	15.77	29	21.54	-	
5213	126	1.03	21.13	15.78	29	21.54	-	
5214	133	-2.18	-78.78	15.79	29	21.68	-	
5214	137	-4.4	-78.79	15.8	29	21.68	-	
5224	127	2.49	0.75	15.69	29	23.01	+	
5224	128	1.92	0.75	15.69	29	23.01	+	
5224	151	-10.51	0.66	15.74	29	23.01	+	
5224	152	-11.04	0.65	15.74	29	23.01	+	
5225	142	-5.22	-99.49	15.7	29	23.14	+	
5225	158	-13.61	-99.56	15.74	29	23.14	+	
5225	159	-14.13	-99.56	15.74	29	23.14	+	
5225	161	-15.14	-99.57	15.74	29	23.14	+	
5225	164	-16.6	-99.58	15.75	29	23.14	+	
5225	168	-18.58	-99.59	15.76	29	23.14	+	
5225	169	-19.07	-99.6	15.76	29	23.14	+	
5225	174	-21.43	-99.61	15.77	29	23.14	+	
5231	1	-0.79	19.79	15.6	29	23.94	+	
5231	3	-1.9	19.78	15.6	29	23.94	+	
5231	5	-2.99	19.78	15.61	29	23.94	+	
5231	9	-5.17	19.76	15.62	29	23.94	+	
5231	11	-6.24	19.75	15.62	29	23.94	+	
5231	14	-7.78	19.73	15.63	29	23.94	+	
5231	15	-8.31	19.73	15.63	29	23.94	+	
5231	17	-9.36	19.72	15.63	29	23.94	+	

5231	18	-9.88	19.71	15.64	29	23.94	+	
5231	20	-10.92	19.7	15.64	29	23.94	+	
5231	21	-11.44	19.7	15.64	29	23.94	+	
5231	22	-11.96	19.69	15.64	29	23.94	+	
5231	23	-12.47	19.69	15.65	29	23.94	+	
5232	147	-6.83	-80.05	15.63	29	24.07	+	
5239	137	0.06	-60.14	15.56	29	25	+	
5242	119	11.04	-0.65	15.46	29	25.4	+	
5242	120	10.47	-0.66	15.46	29	25.4	+	
5243	151	-6.47	-100.61	15.54	29	25.53	-	
5243	158	-10.05	-100.65	15.55	29	25.53	-	
5249	135	3.72	18.6	15.41	29	26.32	-	
5249	144	-1.16	18.57	15.43	29	26.32	-	
5250	144	-1.11	-81.18	15.44	29	26.45	-	
5250	158	-8.39	-81.25	15.47	29	26.45	-	
5250	159	-8.9	-81.26	15.47	29	26.45	-	
5250	160	-9.41	-81.26	15.47	29	26.45	-	
5250	161	-9.92	-81.27	15.47	29	26.45	-	
5257	139	2.63	-61.56	15.36	29	27.38	+	
5267	134	6.74	17.35	15.22	29	28.69	+	
5267	143	1.86	17.31	15.24	29	28.69	+	
5267	145	1.32	17.31	15.24	29	28.69	+	
5303	156	1.6	15.05	14.91	29	33.39	-	
5303	171	-5.81	14.95	14.94	29	33.39	-	
5303	172	-6.29	14.94	14.94	29	33.39	-	
5321	138	-3.37	14.01	14.78	29	35.72	+	
7529	156	9.76	-5.28	13.4	30	10	-	
7529	159	8.46	-5.32	13.4	30	10	-	
7529	160	8.04	-5.33	13.41	30	10	-	
7529	163	6.72	-5.37	13.41	30	10	-	
7529	164	6.32	-5.38	13.41	30	10	-	
7529	177	0.99	-5.56	13.44	30	10	-	
7529	178	0.62	-5.58	13.44	30	10	-	

7561	136	1.14	7.96	13.21	30	14.42	-	
7561	137	0.63	7.96	13.22	30	14.42	-	
7561	139	-0.33	7.96	13.22	30	14.42	-	
7561	141	-1.3	7.96	13.23	30	14.42	-	
7561	143	-2.26	7.96	13.23	30	14.42	-	
7643	199	-4.71	18.07	12.52	30	25.51	-	
7643	200	-5.11	18.07	12.53	30	25.51	-	
7643	201	-5.56	18.08	12.53	30	25.51	-	
7643	202	-5.96	18.08	12.53	30	25.51	-	
7668	26	-7.07	14.8	12.18	30	28.83	+	
7668	27	-7.31	14.78	12.18	30	28.83	+	
7668	34	-8.89	14.65	12.19	30	28.83	+	
10690	96	-8.89	-26.77	14.19	31	114.51	?	
10690	98	-7.98	-26.8	14.2	31	114.51	?	
10690	118	0.54	-27.13	14.23	31	114.51	?	
13050	124	-3.38	-17.16	11.2	32	114.62	?	
13050	125	-3.08	-17.19	11.2	32	114.62	?	
13050	126	-2.78	-17.21	11.2	32	114.62	?	
13050	133	-0.64	-17.36	11.21	32	114.62	?	
13050	134	-0.34	-17.38	11.21	32	114.62	?	

703

704

705

(a)

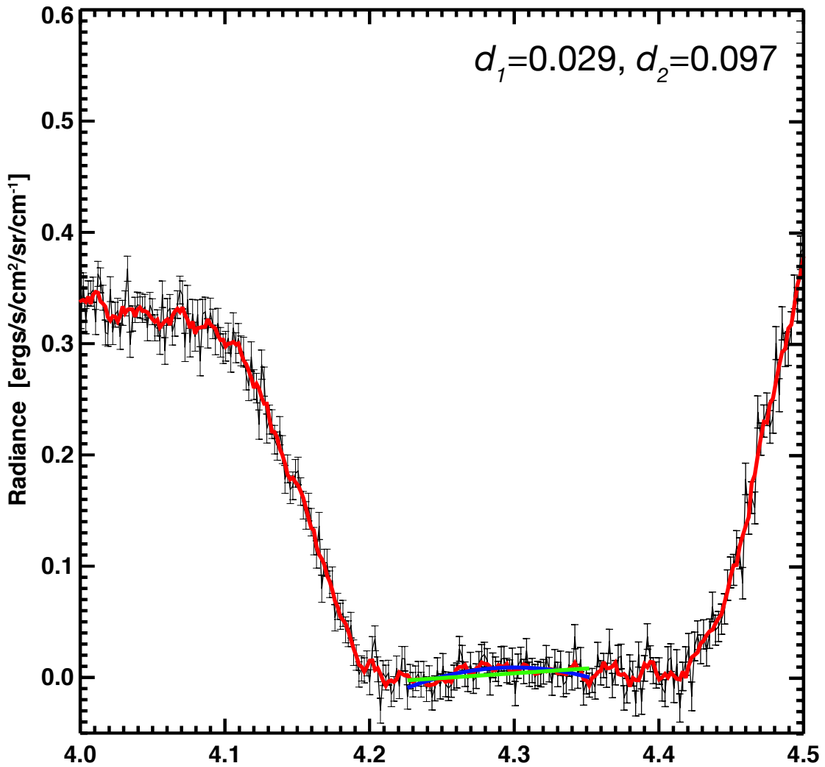
d_1=0.029, d_2=0.097
Radiance [ergs/s/cm²/sr/cm⁻¹]
Wavelength [μm]

(b)

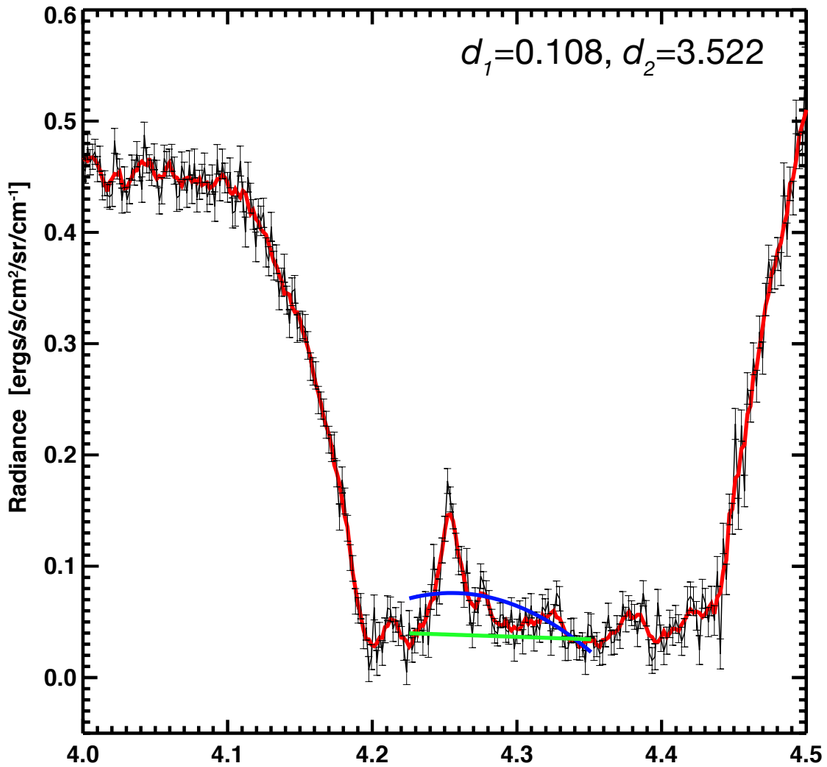
d_1=0.108, d_2=3.522
Radiance [ergs/s/cm²/sr/cm⁻¹]
Wavelength [μm]

(c)

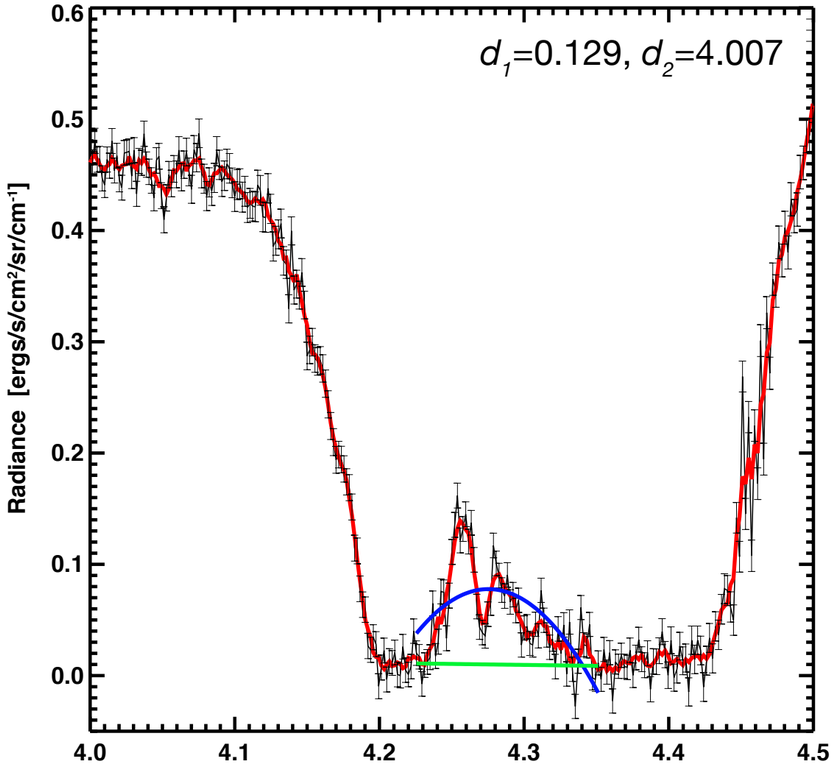
d_1=0.129, d_2=4.007
Radiance [ergs/s/cm²/sr/cm⁻¹]
Wavelength [μm]

(d)

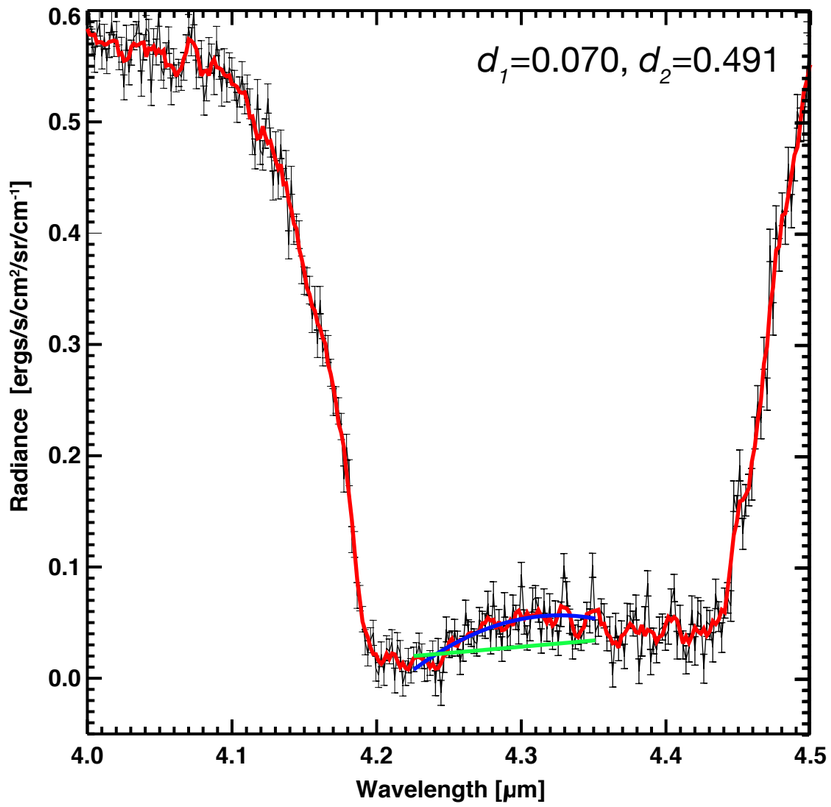
d_1=0.070, d_2=0.491
Radiance [ergs/s/cm²/sr/cm⁻¹]
Wavelength [μm]

(e)

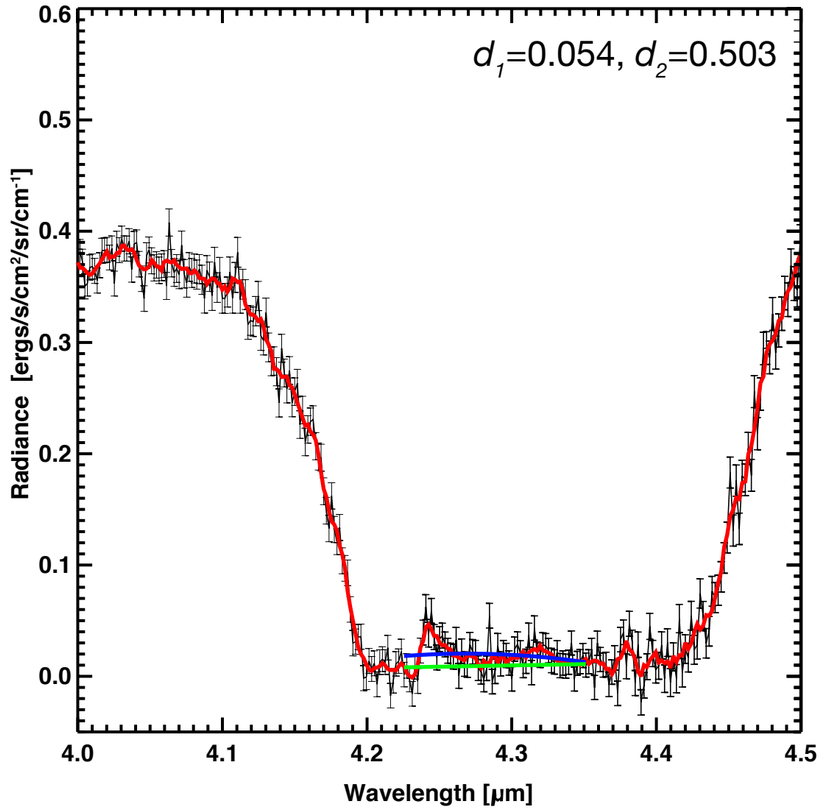
d_1=0.054, d_2=0.503
Radiance [ergs/s/cm²/sr/cm⁻¹]
Wavelength [μm]

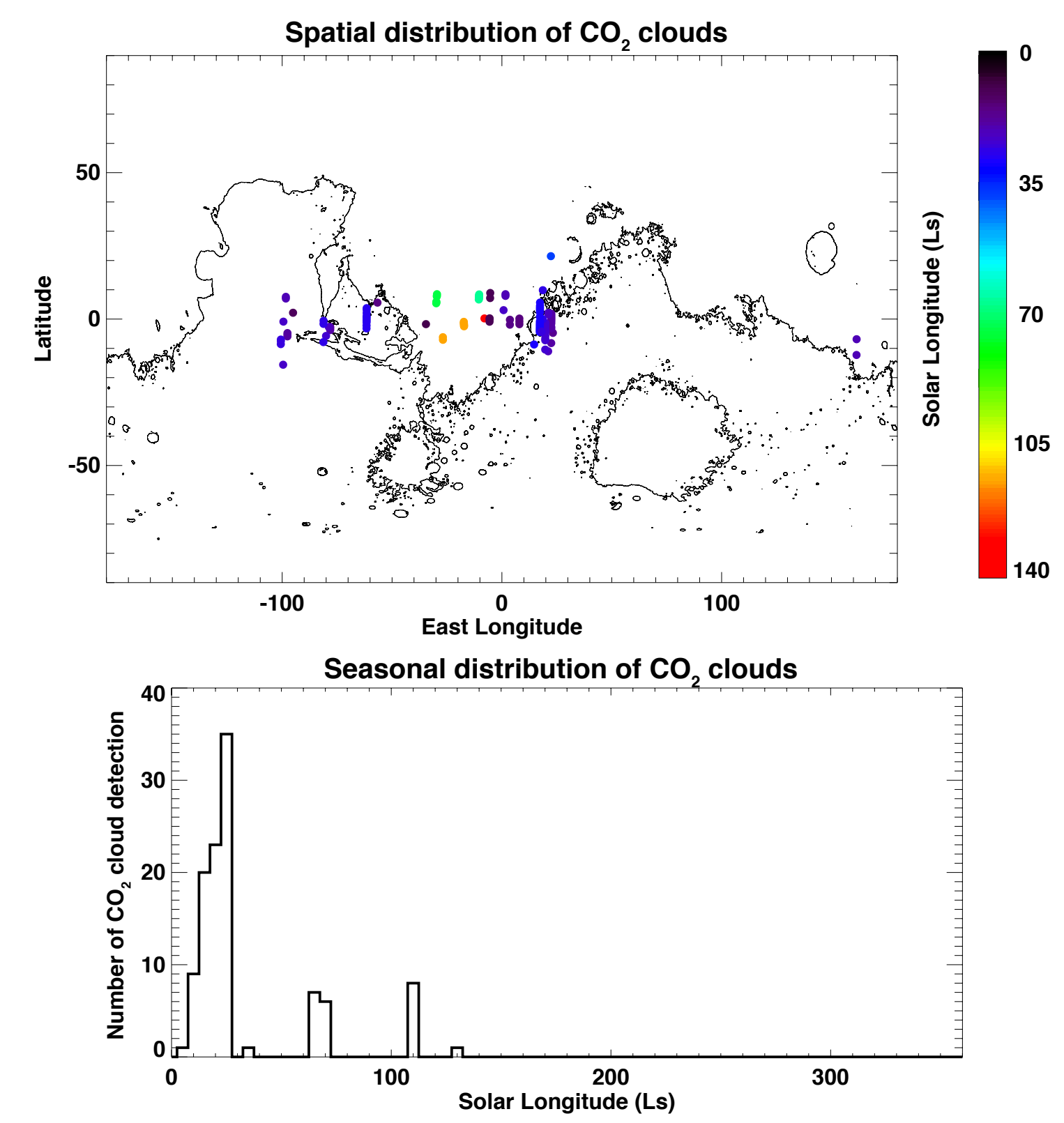
Spatial distribution of CO2 clouds
50
0
-50
Latitude
-100
0
100
East Longitude
Solar Longitude (Ls)
0
35
70
105
140
Seasonal distribution of CO2 clouds
40
30
20
10
0
Number of CO2 cloud detection
0
100
200
300
Solar Longitude (Ls)

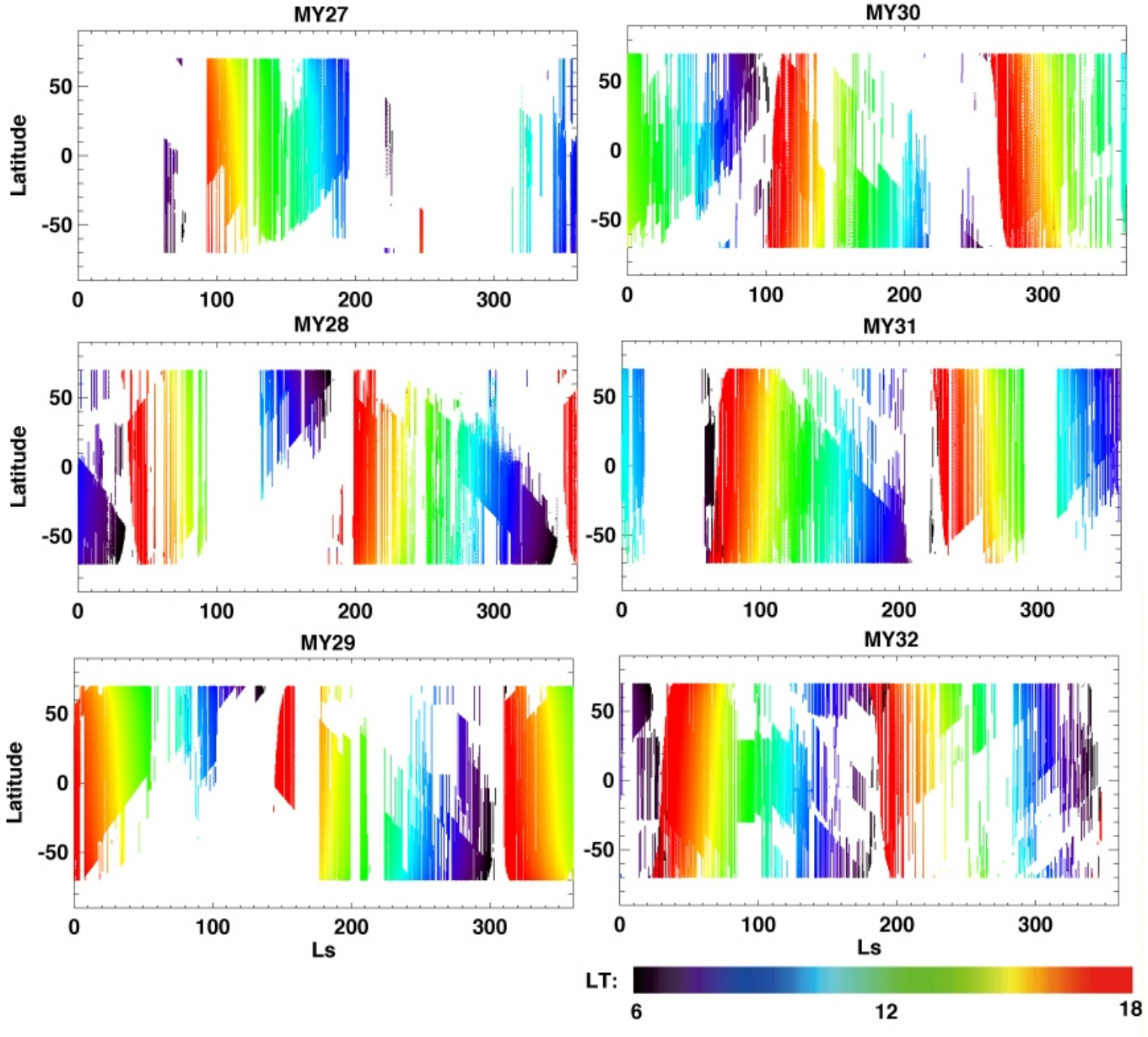
MY27
MY30
MY28
MY31
MY29
MY32
Latitude
Ls
50
0
-50
0
100
200
300
LT:
6
12
18

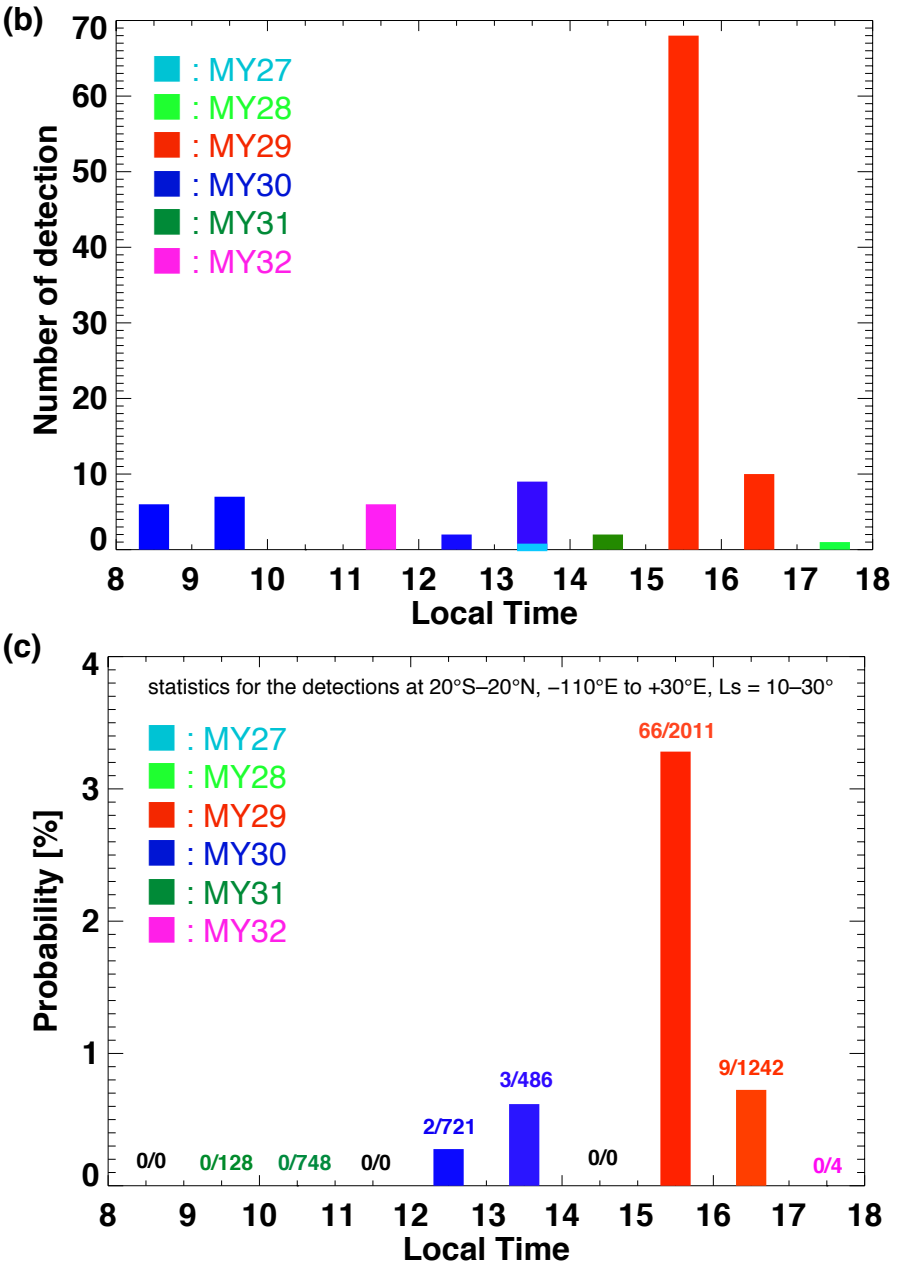
(b)
: MY27
: MY28
: MY29
: MY30
: MY31
: MY32
Number of detection
0
10
20
30
40
50
60
70
8
9
10
11
12
13
14
15
16
17
18
Local Time
(c)
statistics for the detections at 20°S–20°N, −110°E to +30°E, Ls = 10–30°
: MY27
: MY28
: MY29
: MY30
: MY31
: MY32
Probability [%]
0
1
2
3
4
0/0
0/128
0/748
0/0
2/721
3/486
0/0
66/2011
9/1242
0/4
8
9
10
11
12
13
14
15
16
17
18
Local Time

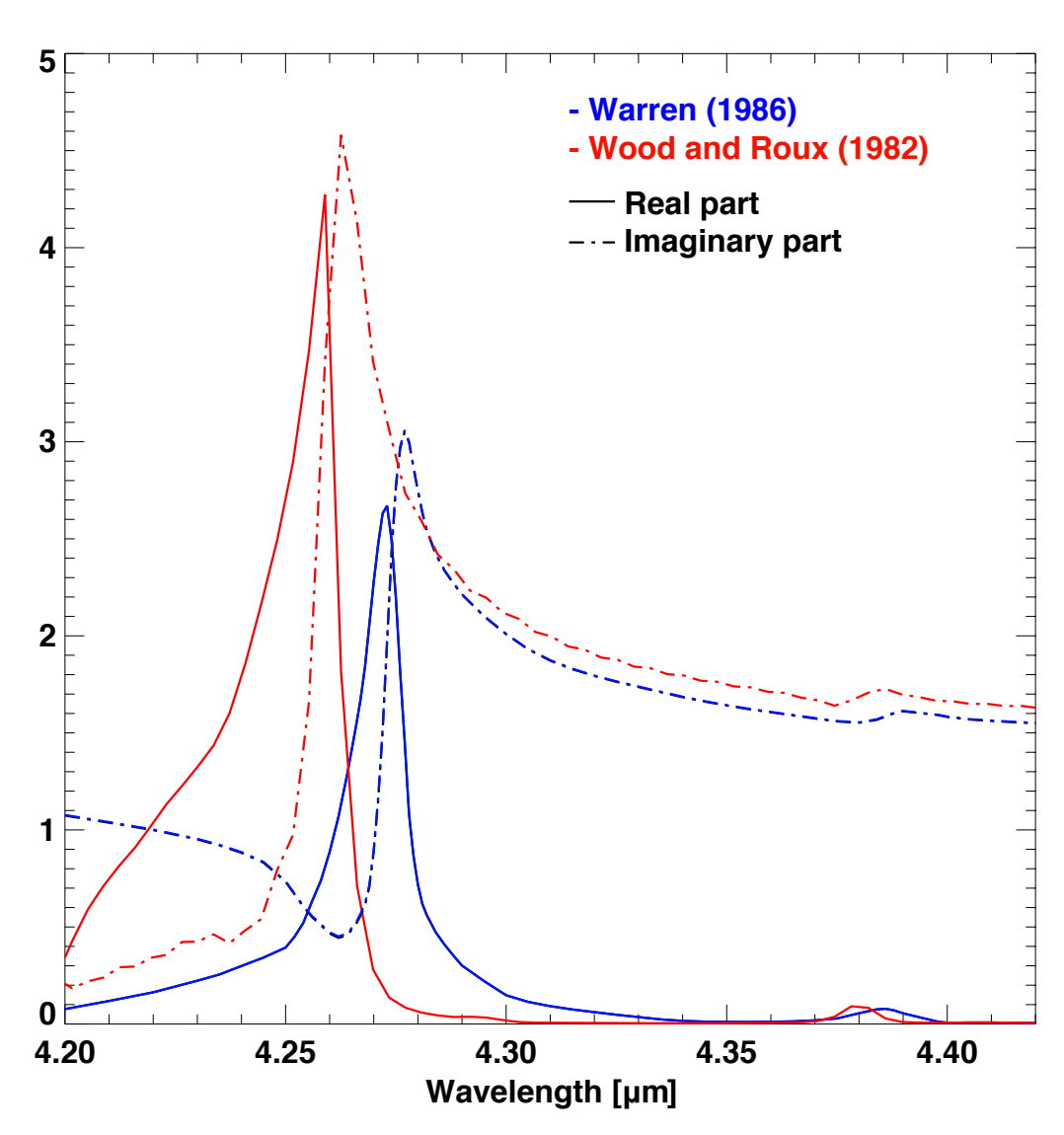
- Warren (1986)
- Wood and Roux (1982)
Real part
Imaginary part
5
4
3
2
1
0
4.20
4.25
4.30
4.35
4.40
Wavelength [μm]

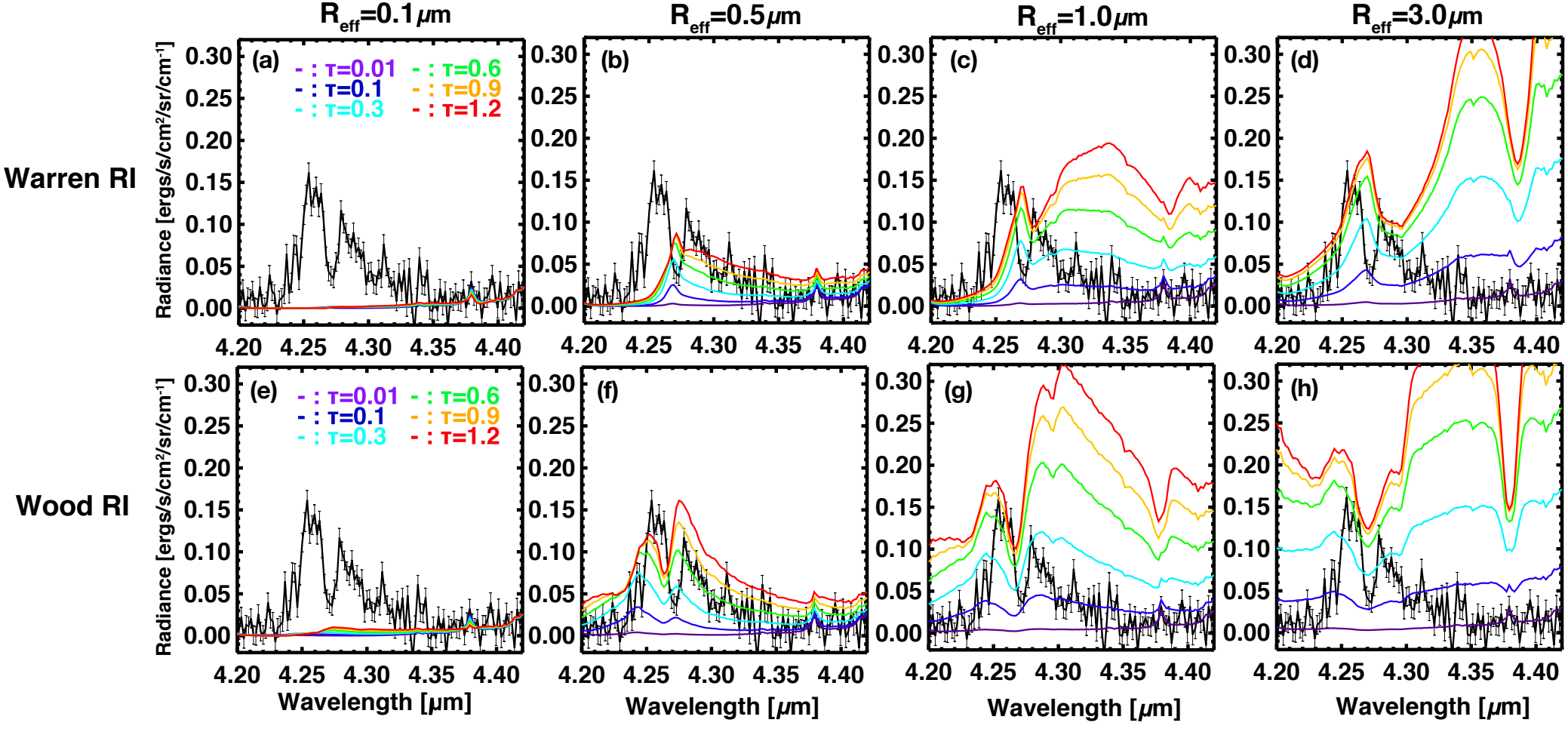
R_eff=0.1μm
R_eff=0.5μm
R_eff=1.0μm
R_eff=3.0μm
Warren RI
Wood RI
(a)
(b)
(c)
(d)
(e)
(f)
(g)
(h)
τ=0.01
τ=0.1
τ=0.3
τ=0.6
τ=0.9
τ=1.2
Radiance [ergs/s/cm²/sr/cm⁻¹]
Wavelength [μm]
0.00
0.05
0.10
0.15
0.20
0.25
0.30
4.20
4.25
4.30
4.35
4.40

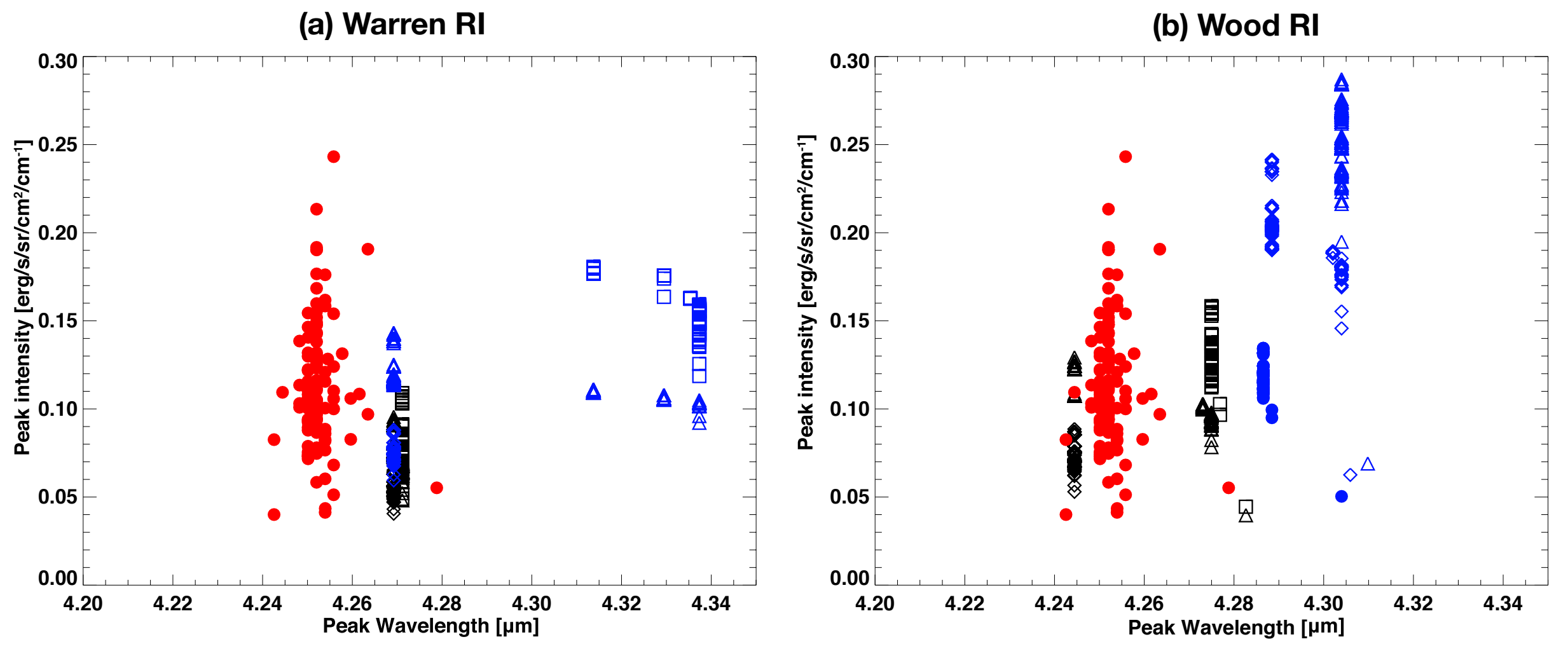
(a) Warren RI
(b) Wood RI
Peak intensity [erg/s/sr/cm²/cm⁻¹]
Peak Wavelength [μm]
0.00
0.05
0.10
0.15
0.20
0.25
0.30
4.20
4.22
4.24
4.26
4.28
4.30
4.32
4.34

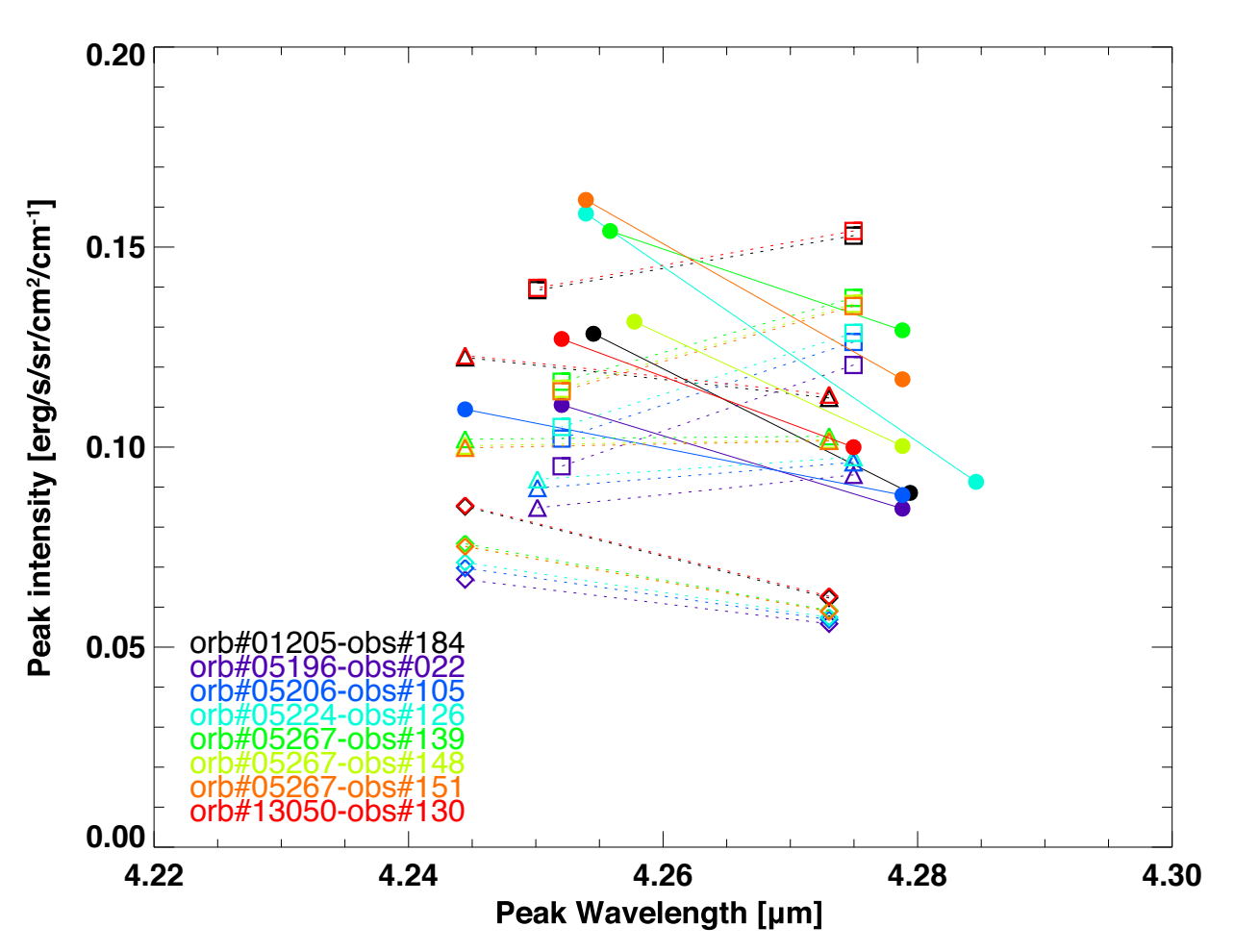
0.20
0.15
0.10
0.05
0.00
Peak intensity [erg/s/sr/cm²/cm⁻¹]
4.22
4.24
4.26
4.28
4.30
Peak Wavelength [μm]
orb#01205-obs#184
orb#05196-obs#022
orb#05206-obs#105
orb#05224-obs#126
orb#05267-obs#139
orb#05267-obs#148
orb#05267-obs#151
orb#13050-obs#130

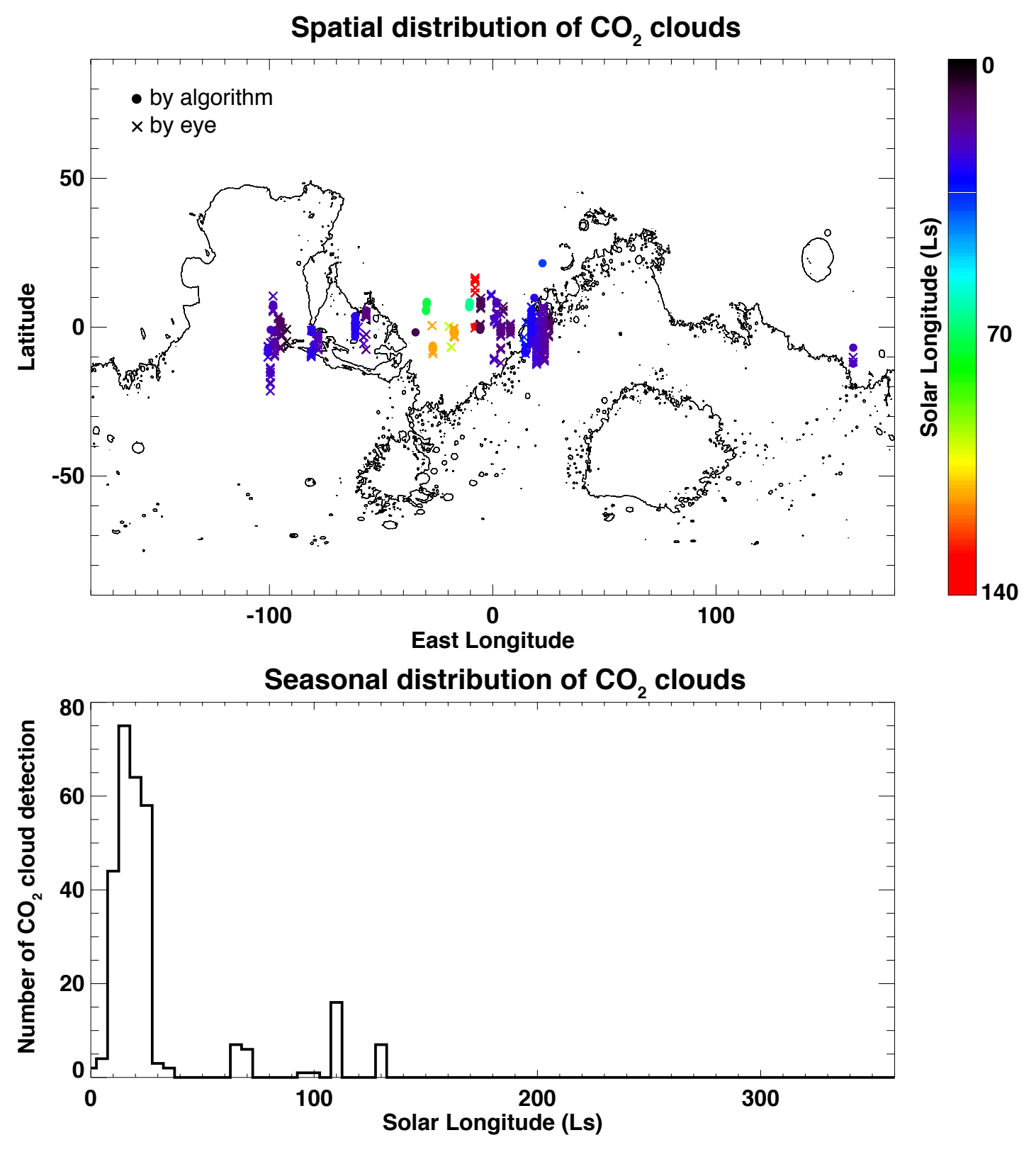
Spatial distribution of CO2 clouds
● by algorithm
× by eye
50
0
-50
Latitude
-100
0
100
East Longitude
0
70
140
Solar Longitude (Ls)
Seasonal distribution of CO2 clouds
80
60
40
20
0
Number of CO2 cloud detection
0
100
200
300
Solar Longitude (Ls)